2. Ha-ras and trk A expression in NBs

We first reported that the Ha-ras expression associated closely with the clinical outcome of the patients [5,6]. The expression is evaluated immunohistochemically and the specific antibody to Ha-ras p21 was originally developed against a peptide of the C-terminal region [5,7]. Recently, a commercial antibody [Ha-ras(C-20), Santa Cruz, CA, USA] is available with same specificity to our antibody. We reported that the immunohistochemical expression of trk A also associated closely with clinical outcome of the patients [8] and was independent from the Ha-ras expression. Moreover, the combination of Ha-ras and trk A expression was useful to discriminate biological behavior of NBs [3]. Both Ha-ras and trk A genes associate closely with differentiation and apoptosis mechanism in NB cells, however, they function in different ways to cell death [9,10].

3. Evaluation of specificity and sensitivity of markers to clinical outcome

We focused the three markers, MYCN gene status, histopathology according to International Neuroblastoma Pathological Classification (INPC) [11] and Ha-ras/trk A expression for predicting clinical outcome of the patients [12]. First we evaluated retrospectively their predictive specificity and sensitivity to the clinical outcome (Fig. 1). The objective patients were diagnosed clinically (non-mass); 45 patients had clinical events such as progress, relapse and/or death and 42 were event-free survivors for more than 2 years after the diagnosis. Specificity to the poor clinical outcome was 86%(19/22) in NBs with MYCN amplification, 76%(25/33) in NBs with INPC unfavorable histology, and 75% (27/36) in NBs with low Ha-ras/trk A expression. However, the sensitivity to all 45 cases with poor clinical outcome were 42%(19/45), 55%(25/45), 60%(27/45) in NBs with MYCN amplification, INPC unfavorable histology and in low Ha-ras/trk A expression, respectively. Prognostic prediction by using one marker was insufficient because of the low sensitivity.

Therefore the three markers were combined for predicting risk to progress. NBs with any of the three markers, MYCN amplification, INPC unfavorable histology or low Ha-ras/trk A expression, increased the sensitivity to poor clinical outcome of the patients to 84% (38/45) and the specificity to poor clinical outcome was 73% (38/52).

On the other hand, NBs with all of three markers, such as 'single copy of MYCN' and 'INCP favorable histology' and 'high Ha-ras/trk A expression', showed quite favorable outcome of the patients. The specificity of the NBs to the good clinical outcome was 88%(22/25). We could predict the risk with high sensitivity and specificity.

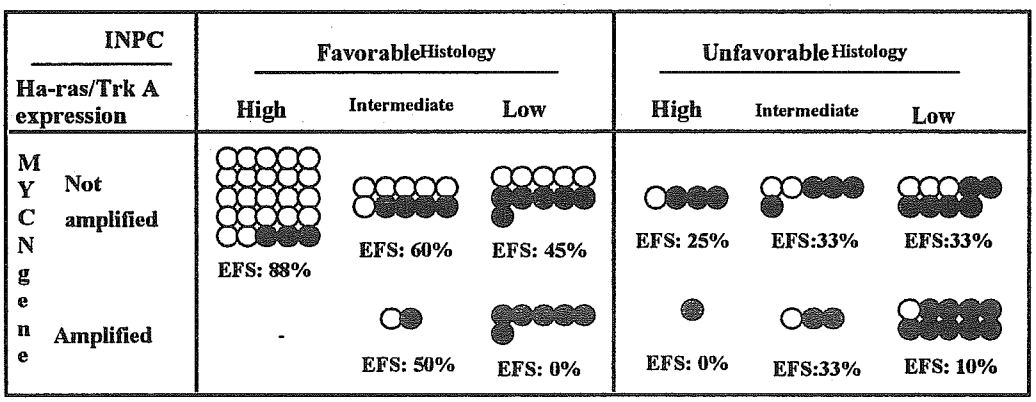

Fig. 1. Clinical outcome of the patients with neuroblastoma. All neuroblastomas were diagnosed clinically (non-massNBs). Open circle presents an event-free survivor and closed circle presents a patient with clinical events, such as death, relapse and progress. *Abbreviations*: INPC, International Neuroblastoma Pathological Classification; EFS, event-free survival rate.

4. Intervention in early stages salvages the patients with risk to progress

In our data base there were 94 NBs with at least one of the risk markers mentioned above. The event-free survival of the patients was 43% (40/94). Even with the cytogenetic markers, event-free survival was 86% in the patients with the localized NBs (stage I or II). On the other hand, the survival was 35% in the patients with advanced NBs (stage III, IVs or IV). This finding reveals that intervention in early stages improves clinical outcome of the patients, even if the NBs have risk to progress.

5. Clinical risk of the NBs defined by multivariate markers

Based on the results mentioned above, the '*high risk*' is defined by NBs in any stage with any of following markers, MYCN amplification or INPC unfavorable histology or low Ha-ras/trk A expression. The '*low risk*' is defined by NBs with all another markers, single copy of MYCN and INPC favorable histology and high Ha-ras/trk A expression and localized tumor. The remaining NBs are defined in '*intermediate risk*' category.

6. Estimation of biological profile in NBs detected through infantile mass-screening program

The Japanese mass-screening program was introduced in 1984 for infants at 6 months of age. This program detected 2366 NBs (mass-NBs) until 2001. The event-free survival of patients is 98%. There have been controversial discussion about benefit of the mass-screening. Quebec [13] and German [14] studies reported that the mass-screening provided no effect on mortality caused by NBs. Recent Japanese nation-wide study showed significant reduction of mortality in mass-screening group comparing with children who did not have the mass-screening [15]. The biological analysis of the mass-NBs has not been conclusive. We have been evaluating the biological property of the 248 mass-NBs and following their clinical outcome. They were about 10% of all mass-NBs in Japan. Based on criteria in the

INPC[a] & Ha-ras/trk A[b] Stage	"Favorable"[a] "High" / "Intermediate" / "Low"[b]			"Unfavorable"[a] "High" / "Intermediate" / "Low"[b]			total□ (EFS/UO)[c]
I	⑩○○○ ○○○○○○ ○○▼▼ n n	○○○○○○ ○○○○n	○○○○ ○▲▼▼ n	○		○○○	99□ (94/5)
II	○○○○ ○○▲▼ n	○○○○ ○○○▲▼	○	○○▼	○○	○	78□ (73/5)
IVs	○○○○○ ○○N	○○○○	○				12□ (12/0)
III	○○ ○n▼	○ ▲●n	○○○○○ ○○○▼ n	○○		▼	46□ (41/5)
IV	○○○○○ ○	○○			●N	○▲▲● N NN	13□ (9/4)
total□ (EFS/UO)[c]	138□ (133/5)	55□ (51/4)	36□ (32/4)	6□ (5/1)	4□ (3/1)	9□ (5/4)	248□ (229/19)

Fig. 2. Biological profiles of 248 mass-NBs. (a) International neuroblastoma pathological classificaion (INPC), (b) H-ras/trk A expression, c; number of event-free survival (EFS) and patients with unfavorable outcome (UO). *Patients outcome*: small open circle presents a event-free survivor and large one presents 10 event-free survivors. Closed circle is a deceased case. A downward closed triangle is a case with relapse NB and a upward closed triangle is a case with progressive NB. Capital 'N' presents MYCN amplification with more than 10 copies and small 'n' presents the amplification with 3–9 copies.

non-mass NBs mentioned above, the 248 mass-NBs were classified into risk categories. Seventy-one percent of them were detected as localized tumors (stage I and II) and 29% were in stages III, IVs and IV. The MYCN amplification was detected in only 13 mass-NBs (5%). The distribution of mass-NBs with MYCN amplification and the better event-free survival [69% (9/13)] of the patients might suggest the benefit of early detection and intervention through the mass-screening. Total 62 NBs (25%) were evaluated to have high-risk property; 55 had INPC unfavorable histology or low Ha-ras/trk A expression and seven had only the MYCN amplification as a risk marker. Among localized 103 NBs (stages I, II) with INPC favorable histology and high Ha-ras/trk A expression, 100 NBs (40%) were classified as *low-risk property* and the MYCN amplified 3 NBs moved to high risk group. The remaining 86 NBs (35%) in other categories were classified to be *Intermediate risk* (Fig. 2).

7. Conclusion

The multivariate evaluation showed the diversity of non-mass- and mass-NBs with variety risk to progress. The cytogenetic markers, MYCN, INPC histology and Ha-ras/trk A expression could predict the risk with high sensitivity and specificity.

Acknowledgements

This study was supported by Grants-in-aid for Cancer Research (13–19, 16–17) and for Scientific Research (H16-Clinical Cancer Research-039) from the Ministry of Health, Labor and Welfare of Japan and by grants (14370250,15659249) from the Ministry of Education, Science, Sports and Culture

References

[1] J.M. Maris, K.K. Matthay, Molecular biology of neuroblastoma, J. Clin. Oncol. 17 (1999) 2264–2279.
[2] R.C. Seeger, G.M. Brodeur, H. Sather, A. Dalton, S.E. Siegel, K.Y. Wong, D. Hammond, Association of multiple copies of the N-myc oncogene with rapid progression of neuroblastgomas, N. Engl J. Med. 313 (1985) 1111–1116.
[3] T. Tanaka, T. Sugimoto, T. Sawada, Prognostic discrimination among neuroblastomas according to Ha-ras/trk A gene expression, Cancer 83 (1998) 1626–1633.
[4] G.M. Brodeur, Neuroblastoma: biological insights into a clinical enigma, Nat. Rev. Cancer 3 (2003) 203–216.
[5] T. Tanaka, D.J. Slamon, H. Shimoda, C. Waki, Y. Kawaguchi, Y. Tanaka, N. Ida, Expression of Ha-ras oncogene products in human neuroblastomas and significant correlation with patient's prognosis, Cancer Res. 48 (1988) 1030–1034.
[6] T. Tanaka, D.J. Slamon, H. Shimada, H. Shimoda, T. Fujisawa, N. Ida, R.C. Seeger, A significant association of Ha-ras p21 in neuroblastoma cells with patient prognosis, Cancer 68 (1991) 1296–1302.
[7] T. Tanaka, D.J. Slamon, M.J. Cline, Efficient generation of antibodies to oncoproteins by using synthetic peptide antigens, Proc. Natl Acad. Sci. USA 82 (1985) 3400–3404.
[8] T. Tanaka, E. Hiyama, T. Sugimoto, T. Sawada, M. Tanabe, N. Ida, Trk A gene expression in neuroblastoma: the clinical significance of an immunohistochemical study, Cancer 76 (1995) 1086–1095.
[9] A. Nakagawara, M. Arima-Nakagawara, N.J. Scavarda, C.G. Azar, A.B. Canter, G.M. Brodeur, Association between high levels of expression of the trk gene and favorable outcome in human neuroblastoma, N. Engl J. Med. 328 (1993) 847–854.
[10] C. Kitanaka, K. Kato, R. Ijiri, K. Sakurada, A. Tomiyama, K. Noguchi, et al., Increased ras expression and caspase-independent neuroblastoma cell death: possible mechanism of spontaneous neuroblastoma regression, J. Natl Cancer Inst. 94 (2002) 358–368.
[11] H. Shimada, I. Ambros, L.P. Dehner, J. Hata, V.V. Joshi, B. Roald, et al., The international neuroblastoma pathology classification (the Shimada system), Cancer 86 (1999) 364–372.
[12] T. Tanaka, T. Iehara, T. Sugimoto, M. Hamasaki, S. Teramukai, Y. Tsuchida, et al., in: B. De Bernardi, A. Garaventa et al. (Eds.), Multivariate evaluation for heterogeneous neuroblastomas Advances in Neuroblastoma Research, Eleventh Conference, Genova (2004), p. 64.
[13] W.G. Wood, R.M. Gao, J.J. Shuster, L.L. Robinson, M. Bernstein, S. Weitzman, et al., Lemieux: Screening of infants and mortality due to neuroblastoma, N. Engl J. Med. 346 (2002) 1041–1046.
[14] F.H. Schilling, C. Spix, F. Berthold, R. Erttmann, N. Fehse, B. Hero, et al., Neuroblastoma screening at one year of age, N. Engl J. Med. 346 (2002) 1047–1053.
[15] K. Hayashi, T. Fujita, K. Katanoda, T. Sobue, M. Nishi, K. Yamamoto, in: B. De Bernardi, A. Garaventa et al. (Eds.), Effectiveness of Mass-screening program on neuroblastoma mortality in 1995–2000 birth cohort of Japan: nationwide neuroblastoma mortality study Advances in Neuroblastoma Research, Eleventh Conference, Genova (2004), p. 93.

CpG Island Methylator Phenotype Is a Strong Determinant of Poor Prognosis in Neuroblastomas

Masanobu Abe,[1,2] Miki Ohira,[3] Atsushi Kaneda,[1] Yukiko Yagi,[1] Seiichiro Yamamoto,[4] Yoshihiro Kitano,[5] Tsuyoshi Takato,[2] Akira Nakagawara,[3] and Toshikazu Ushijima[1]

[1]Carcinogenesis Division, National Cancer Center Research Institute; [2]Department of Oral and Maxillo Facial Surgery, University of Tokyo Graduate School of Medicine; [3]Biochemistry Division, Chiba Cancer Center Research Institute; [4]Information Division, Research Center for Cancer Prevention and Screening, National Cancer Center; and [5]Department of Pediatric Surgery, National Center for Child Health and Development, Tokyo, Japan

Abstract

Neuroblastoma, one of the most common pediatric solid tumors, is characterized by two extreme disease courses, spontaneous regression and life-threatening progression. Here, we conducted a genome-wide search for differences in DNA methylation that distinguish between neuroblastomas of the two types. Three CpG islands (CGI) and two groups of CGIs were found to be methylated specifically in neuroblastomas with a poor prognosis. By quantitative analysis of 140 independent cases, methylation of all the five CGI (groups) was shown to be closely associated with each other, conforming to the CpG island methylator phenotype (CIMP) concept. The presence of CIMP was sensitively detected by methylation of the *PCDHB* CGIs and associated with significantly poor survival (hazard ratio, 22.1; 95% confidence interval, 5.3-93.4; $P < 0.0001$). Almost all cases with N-*myc* amplification (37 of 38 cases) exhibited CIMP. Even in 102 cases without N-*myc* amplification, the presence of CIMP (30 cases) strongly predicted poor survival (hazard ratio, 12.4; 95% confidence interval, 2.6-58.9; $P = 0.002$). Methylation of *PCDHB* CGIs, located in their gene bodies, did not suppress gene expression or induce histone modifications. However, CIMP was significantly associated with methylation of promoter CGIs of the *RASSF1A* and *BLU* tumor suppressor genes. The results showed that neuroblastomas with CIMP have a poor prognosis and suggested induction of silencing of important genes as an underlying mechanism. (Cancer Res 2005; 65(3): 828-34)

Introduction

Epigenetic abnormalities, especially alterations in DNA methylation, are intimately involved in development of various human tumors (1). Aberrant methylation of promoter CpG islands (CGI) causes inactivation of tumor suppressor genes. Genomic instability is caused by genomic hypomethylation and is associated with hypermethylation (2, 3). Identification of epigenetic abnormalities in human cancers is expected to lead not only to discovery of novel disease mechanisms but also to development of new diagnostic markers. Therefore, we previously developed a genome-wide scanning method, methylation-sensitive representational difference analysis (MS-RDA), for detecting differences in DNA methylation (4, 5). This technique analyzes unmethylated, CpG-rich regions of the genome and has already identified genes silenced in human lung, stomach, breast, and pancreatic cancers (6–9).

Neuroblastoma derived from primitive cells of the sympathetic nervous system is one of the most common solid tumors in childhood, characterized by two extreme disease courses, spontaneous regression, and life-threatening progression (10, 11). The clinical outcome is associated with disease stage, age at diagnosis, histologic classification, N-*myc* amplification, DNA ploidy, and *TrkA* overexpression (10–12). These characteristics are therefore used to classify cases into low-, intermediate-, and high-risk groups. However, especially in the cases with intermediate risk, prediction of prognosis and therapeutic decision-making are still difficult, and development of new markers is an urgent priority. Moreover, the molecular bases underlying the two distinct clinical courses are still unknown, and their clarification is needed to allow development of novel therapeutics.

In the present study, considering the major involvement of epigenetic machinery in embryonic development (13, 14), we searched for differences in DNA methylation between neuroblastomas with a good prognosis and counterparts with a poor prognosis by MS-RDA.

Materials and Methods

Tissue Samples and Cell Lines. Tumor samples were obtained from 145 nonrecurrent cases between 1995 and 1999 and were used under approval of institutional review boards. The mean age at initial diagnosis was 27 months (range, 0-216 months). Their clinical stages were determined according to the International Neuroblastoma Staging System, and 40, 17, 20, 60, and 8 cases belonged to stages I, II, III, IV, and IVS, respectively. Normal adrenal medulla tissue was collected from a case undergoing nephrectomy for a renal cancer. Neuroblastoma cell lines were obtained from the American Type Culture Collection (Manassas, VA), the Japanese Collection of Research Bioresources (Tokyo, Japan), and the RIKEN Bio Resource Center (Tsukuba, Japan). GANB was established by A.N. and normal human bronchial epithelial cells were purchased from Cambrex (East Rutherford, NJ). High molecular weight DNA and total RNA were extracted as previously described (7). Total RNAs of brain and adrenal glands were purchased from Clontech (Palo Alto, CA).

MS-RDA and Database Search. MS-RDA was done as previously described (4, 5). Genomic DNA of primary neuroblastomas with a good prognosis (cases 92, 98, 104, 112, and 148) and neuroblastoma cell lines established from cases with a poor prognosis (CHP134, IMR32, GANB, NGP, and TGW) were digested with *Hpa*II, and then two pooled DNA samples were prepared. Although use of cell lines is highly recommended for MS-RDA (5), no cell lines were available for neuroblastomas with a good prognosis, and therefore we used the primary samples. To isolate CGIs that were hypermethylated in the latter, the cell line pool was used as the tester, and the primary tumor pool as the driver. MS-RDA in the opposite direction

Note: Supplementary data for this article are available at Cancer Research online (http://cancerres.aacrjournals.org/).

Requests for reprints: Toshikazu Ushijima, 5-1-1 Tsukiji, Chuo-ku, Tokyo 104-0045, Japan. Phone: 133-547-5240; Fax: 135-565-1753; E-mail: tushijim@ncc.go.jp.

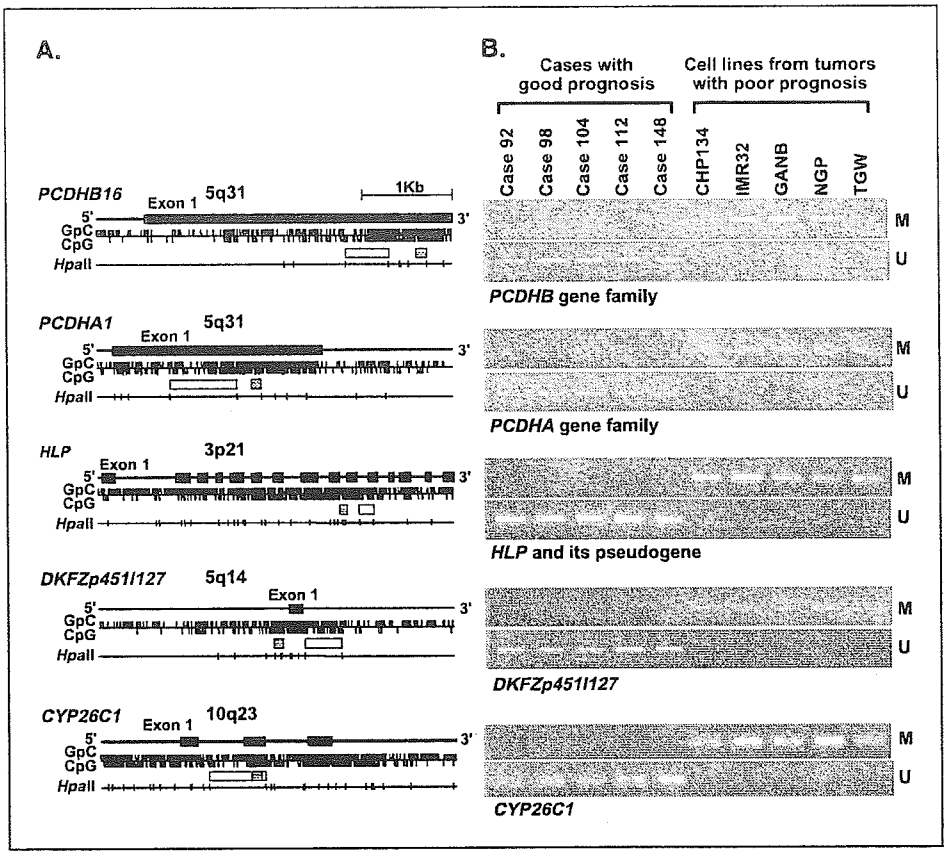

Figure 1. Five CGIs isolated by MS-RDA and their methylation statuses in the samples used for MS-RDA. *A*, genomic structures of the five CGIs. GpC, CpG, and *HpaII* recognition sites (5′-CCGG-3′) are shown by ticks. *Closed boxes*, exons; *open boxes*, clones isolated by MS-RDA; *shaded boxes*, regions analyzed by MSP. *B*, methylation statuses analyzed by MSP. *M*, MSP using primers specific to methylated DNA; *U*, MSP using primers specific to unmethylated DNA. All the five CGIs were found to be differentially methylated between the two groups used for MS-RDA.

was also done. For each series of MS-RDA, 96 clones were analyzed for redundancy, and nonredundant clones were sequenced. Their genomic origins were examined using BLASTN software http://www.ncbi.nlm.nih.gov/BLAST/).

Sodium Bisulfite Modification and Methylation-Specific PCR. One microgram of DNA underwent sodtlbium bisulfite modification (15), and was suspended in 20 μL of TE buffer. For methylation-specific PCR (MSP), 1 μL of the solution was used for PCR with primers specific to methylated or unmethylated sequences. Using DNA from normal human bronchial epithelial and DNA methylated with *SssI* methylase, annealing temperatures specific for methylated and unmethylated primers were determined. Quantitative MSP was done separately for methylated DNA molecules and for unmethylated DNA molecules. Standard DNA was prepared by cloning PCR products amplified by methylated and unmethylated primers into a vector, respectively. The numbers of methylated and unmethylated molecules in a test sample were determined by comparing their amplification with those of standard samples containing 10 to 10^6 molecules. The "methylation index" was calculated as the fraction of methylated molecules in the total DNA molecules (no. methylated molecules + no. unmethylated molecules). Each sample was analyzed twice, blind to clinical information, and high reproducibility was confirmed (correlation coefficient = 0.98).

The *protocadherin* β (*PCDHB*) family consists of 16 genes with single exons and three pseudogenes on 5q31, and their CGIs are located in the gene bodies. MSP primers were designed to recognize 17 of the 19 members (all except for the *PCDHB1* gene and the *PCDHB19* pseudogene). The *protocadherin* α (*PCDHA*) family consists of 15 genes and one pseudogene having unique first exons and shared exons 2 to 4 on 5q31, and their CGIs are located in exon 1. MSP primers were designed to recognize 13 of the 16 members (all except for the *PCDHAC1* and *PCDHAC2* genes and the *PCDHA14* pseudogene). The *hepatocyte growth factor-like protein* (*HLP/MSP/MST1*) gene is highly homologous to *macrophage stimulating, pseudogene 9* (*MSTP9*), and MSP primers were designed to recognize both of these. For *DKFZp451I127*, *FLJ37440*, *Zinc finger protein 297* (*ZNF297*), and *Cytochrome p450 CYP26C1* (*CYP26C1*), MSP primers were designed to recognize each of them specifically. The primers and PCR conditions are shown in Supplementary Table 1.

Semiquantitative and Quantitative Reverse Transcription-PCR. cDNA was synthesized from 3 μg of total RNA treated with DNase using a Superscript II kit (Invitrogen Co., Carlsbad, CA). For semiquantitative reverse transcription-PCR (*PCDHB1-PCDHB15*), multiple cycles of PCR were tested for each gene, and numbers giving a wide dynamic range were determined. The primers and PCR conditions are shown in Supplementary Table 2. For quantitative reverse transcription-PCR (*PCDHB16*), the number of cDNA molecules was determined by quantitative PCR, as in quantitative MSP, and the copy number was normalized to that of *GAPDH*.

Chromatin Immunoprecipitation Assay. From 1×10^6 cells, DNA/histone complexes were immunoprecipitated, and DNA was eluted in 30 μL of TE after reversing cross-linking. Copy numbers of DNA molecules of the *PCDHB16* exon, *RASSF1A* promoter, and *GAPDH* promoter in 1 L of the eluate were determined by quantitative PCR (primer sequences in Supplementary Table 3), and normalized to the copy numbers in the input. Anti-acetyl-histone H3 antibody (AcH3) and anti-dimethylated-histone H3 (lysine 9; MetH3K9) were purchased from Cell Signalling (Beverly, MA).

Statistical Analysis. Associations between methylation levels among CGI groups were examined using the Pearson correlation coefficient and Fisher's exact test. Survival time was measured from the date of initial diagnosis to the date of death or last contact. Kaplan-Meier analysis and log-rank tests were done to compare survival between the groups defined by methylation levels. Hazard ratio (HR) between groups and dose-response relationships between methylation levels and survival were estimated by the Cox proportional hazard model. Kaplan-Meier curves were drawn with the help of Aabel software (Gigawiz. Ltd. Co., Tulsa, OK) and other analyses were conducted using SAS version 8.2 (SAS Institute, Inc., Cary, NC).

Results

Genome-Scanning for Differentially Methylated CpG Islands. MS-RDA was done using five primary neuroblastomas with a good prognosis and five neuroblastoma cell lines established from cases with a poor prognosis. Seven DNA fragments, derived from CGIs of *PCDHB16*, *PCDHA1*, *HLP*, *DKFZp451I127*, *FLJ37440*, *ZNF297*, and *CYP26C1*, were isolated as methylated in the latter samples. No DNA fragments were isolated as methylated in the former samples. Methylation statuses of (i) 17 CGIs of the *PCDHB* family (detailed structure in Supplementary Fig. 1), (ii) 13 CGIs of the *PCDHA* family, (iii) *HLP* and its pseudogene, and (iv) other four unique CGIs were examined by MSP. This revealed that the *PCDHB* family (5q31), the *PCDHA* family (5q31), *HLP* (3p21) and its pseudogene (1p36), *DKFZp451I127* (5q14), and *CYP26C1* (10q23) were specifically methylated in the latter samples (Fig. 1*A* and *B*).

Close Association between Methylation and Poor Prognosis in 140 Independent Primary Samples. To analyze the significance of the differential methylation of the above five CGI (groups) in primary neuroblastomas, 140 primary samples, all different from the initial five samples, were analyzed by quantitative MSP. When distributions of methylation indices were analyzed (Fig. 2), a clear bimodal distribution was observed for (i) the CGI group in the *PCDHB* family (17 CGIs), (ii) the CGIs of *HLP* and its pseudogene, and (iii) the *CYP26C1* CGI. The results thus indicated that the cases could be classified into two groups, one with high methylation and the other with low methylation. The dose-response relationships between high *PCDHB* methylation and poor prognosis were analyzed by the Cox proportional model using the methylation index as a continuous value, and the association was confirmed with a trend $P < 0.0001$. Normal adrenal medulla had a methylation index of 4%.

According to the bimodal distribution, the effect of high methylation was assessed by dichotomous groups. For the *PCDHB* family, cutoff values of 30%, 40%, 50%, 60%, 70%, and 80% were tested, and HRs of 16.8 [95% confidence interval (95% CI), 4.0-70.9], 22.1 (95% CI, 5.3-93.4; Fig. 3), 13.1 (95% CI, 4.5-37.9), 9.1 (95% CI, 3.8-23.4), 7.0 (95% CI, 3.1-15.8), and 7.8 (95% CI, 3.4-17.6), respectively, were obtained ($P < 0.001$ for all cutoff values). This showed that cases can be classified into two groups with distinct prognoses, and we adopted a cutoff value of 40%, which gave the highest HR, for convenience in the following analysis.

The dose-response relationships were also confirmed for other four CGI (groups), *PCDHA* ($P = 0.004$), *HLP* ($P < 0.0001$), *DKFZp451I127* ($P = 0.02$), and *CYP26C1* ($P < 0.0001$). Cutoff values were similarly tested, and those for *PCDHA*, *HLP*, *DKFZp451I127*, and *CYP26C1* were set at 80%, 10%, 20%, and 70%, respectively, with HRs of 5.7 (95%CI, 1.4-24.0; $P = 0.07$), 21.7 (95% CI, 5.1-91.4; $P < 0.0001$), 3.2 (95% CI, 1.0-10.5; $P = 0.045$), and 8.7 (95% CI, 4.1-18.1; $P < 0.0001$), respectively (Fig. 3).

Existence of the CpG Island Methylator Phenotype in Neuroblastomas. Methylation of the different CGI (groups) had shown close associations with each other (Table 1). When correlation was analyzed as a continuous value, Pearson correlation coefficients between *PCDHB* and *PCDHA*, *HLP*, *DKFZp451I127* and *CYP26C1* were 0.55, 0.70, 0.26 and 0.77, respectively. This showed that multiple CGIs were simultaneously methylated in

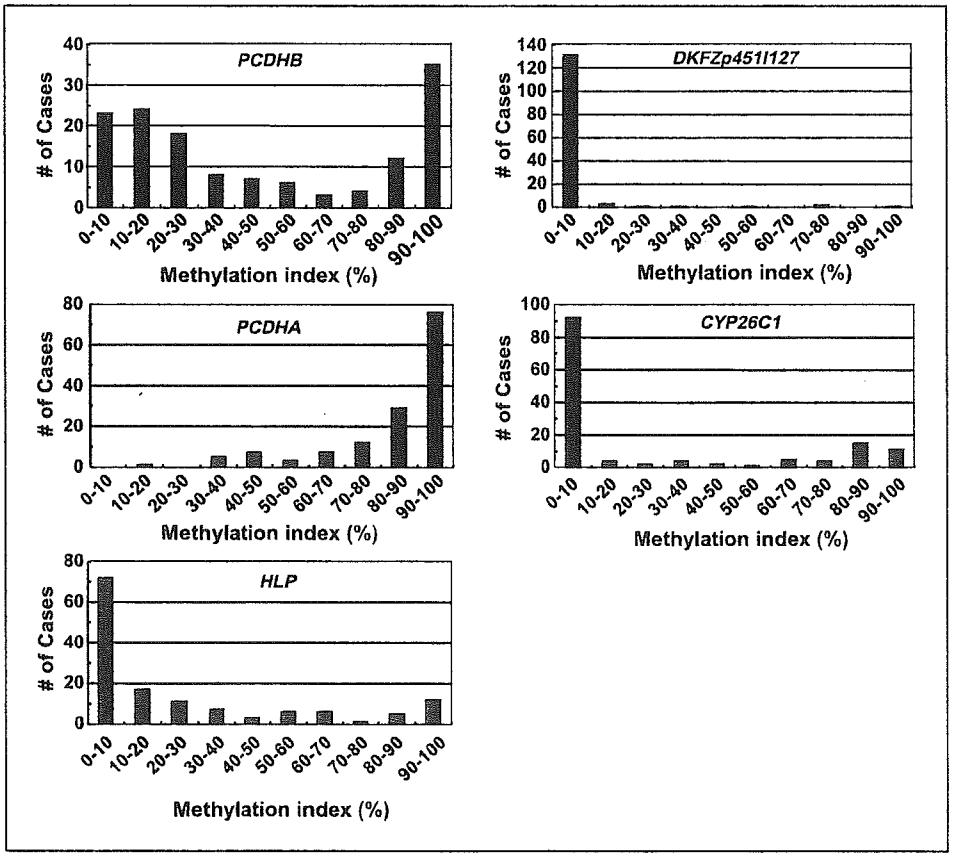

Figure 2. The distribution of methylation indices among the 140 cases analyzed: (*i*) 17 CGIs of the *PCDHB* family, (*ii*) 13 CGIs of the *PCDHA* family, (*iii*) CGIs of *HLP* and its pseudogene, (*iv*) *DKFZp451I127*, and (*v*) *CYP26C1*.

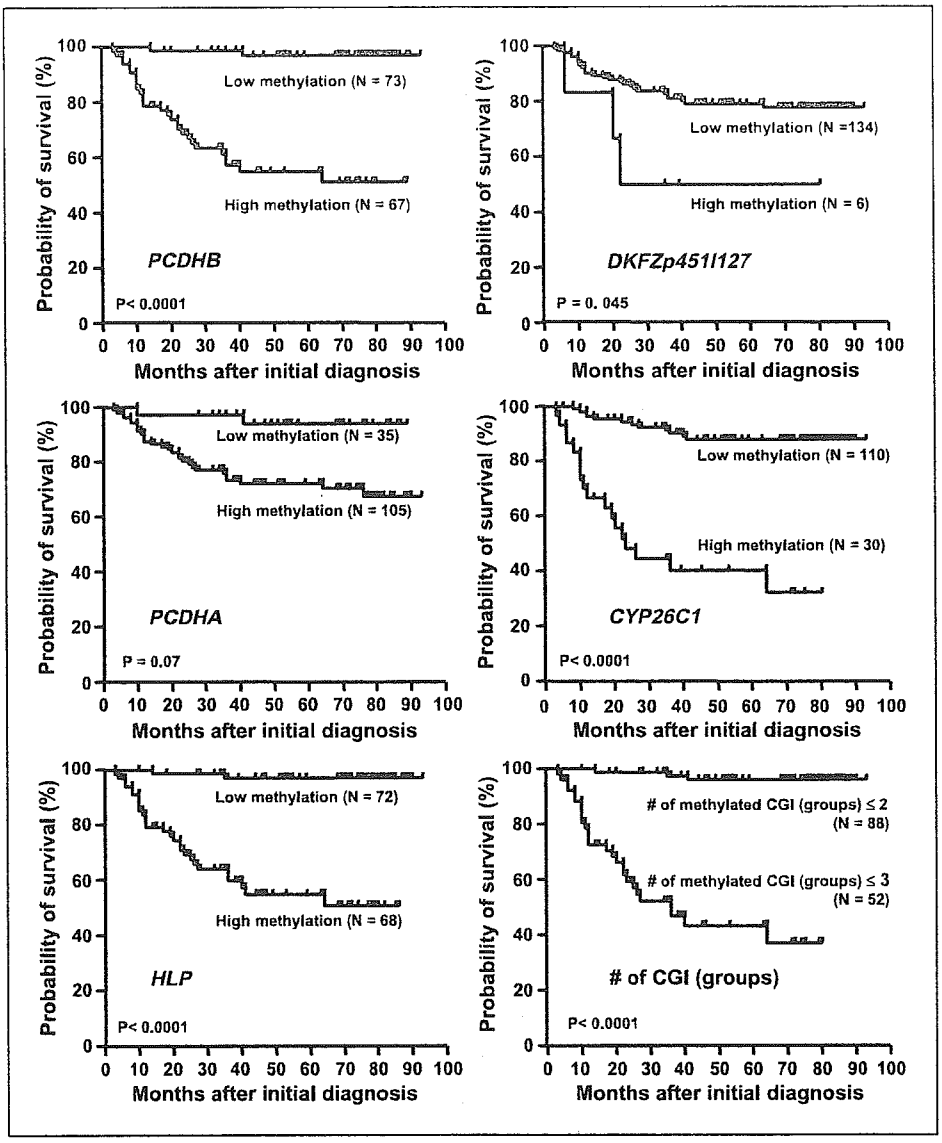

Figure 3. Predictive powers of methylation of the five CGI (groups) identified, and their multiple methylation: (*i*) 17 CGIs of the *PCDHB* family, (*ii*) 13 CGIs of the *PCDHA* family, (*iii*) CGIs of *HLP* and its pseudogene, (*iv*) *DKFZp451I127*, (*v*) *CYP26C1*, and (*vi*) methylation of three of these or more were analyzed by the Kaplan-Meier method using 140 primary samples. The *PCDHB* family, *HLP*, *DKFZp451I127*, *CYP26C1*, and methylation of multiple CGI (groups) had significant influence on survival.

neuroblastomas with a poor prognosis (Supplementary Fig. 2*A*). The simultaneous methylation of (i) 17 CGIs of the *PCDHB* family, (ii) 13 CGIs of the *PCDHA* family, (iii) CGIs of *HLP* and its pseudogene, (iv) *DKFZp451I127* CGI, and (v) *CYP26C1* CGI conformed with the concept of the CpG island methylator phenotype (CIMP; ref. 16).

Associations between CIMP and poor prognosis were examined by defining CIMP as cases with methylation of two CGI (groups) or more, those with three or more, those with four or five, and those with five. When CIMP was defined as cases with methylation of three CGI (groups) or more, the largest association with poor prognosis was observed, with a HR of 25.4 (95% CI, 7.6-84.5; Fig. 3). However, the HR (22.1) given by 17 CGIs of the *PCDHB* gene family approximated to this, and the *PCDHB* methylation level closely correlated with the number of methylated CGI (groups; Supplementary Fig. 2*B*). Therefore, for simplicity of analysis, we defined CIMP in neuroblastomas on the basis of high methylation of the *PCDHB* family, tentatively with a cutoff value of 40%.

Predictive Power of CIMP, Compared with Known Prognostic Factors. Univariate analyses showed that N-*myc* amplification, low *TrkA* expression, DNA diploidy, and an age no younger than 1 year gave HRs of 9.5 (95% CI, 4.4-20.5), 3.9 (95% CI, 1.7-9.3), 4.2 (95% CI, 1.65-10.8), and 12.3 (95% CI, 3.7-41.7). Cases were stratified by these known factors (Table 2). In those without N-*myc* amplification, CIMP also showed an influence with a HR of 12.4 (95% CI, 2.6-58.9), but almost all cases with N-*myc* amplification (37 of the 38 cases) showed CIMP. It was suggested that cases with N-*myc* amplification were contained in the cases with CIMP. CIMP was independent from *TrkA* overexpression, DNA ploidy, and age at diagnosis. Stage seemed to be a stronger prognostic factor. Notably, even when limited to cases in stages III and IV without N-*myc* amplification, which are classified into the intermediate risk group and clinically important, CIMP gave a HR of 4.8 (95% CI, 1.0-23.0; $P = 0.048$).

Multivariate analyses were finally done taking all the five known prognostic factors into account. Although CIMP gave a HR of 5.0 (95% CI, 0.47-52.7), it was not significant ($P = 0.18$), possibly due to limitation in the number of cases.

Table 1. Association between the *PCDHB* methylation and methylation of other CGIs

Variables	Methylation level of *PCDHB* family gene		*P**
	High (≥40%)	Low (<40%)	
No. cases (n = 140)	67	73	
Methylation of CGIs outside promoter regions (n = 140)			
PCDHA gene family (exon 1)†	65/67	41/73	<0.0001
HLP (exons 2-13)‡	52/67	16/73	<0.0001
CYP26C1 (exon 2)§	30/67	0/73	<0.0001
p41Arc (intron 8)	1/67	1/73	0.48
SIM2 (exon 2)	0/67	0/73	
Methylation of CGIs in promoter regions (n = 140)			
DKFZp451I127‖	6/67	0/73	0.011
RASSF1A	51/67	10/73	<0.0001
BLU	25/67	3/73	<0.0001
p16	0/67	0/73	
hMLH1	0/67	0/73	
PCDHB1	0/67	0/73	
TAF7	0/67	0/73	
p41Arc	0/67	0/73	
SIM2	0/67	0/73	

*Fisher's exact test.
†Boundaries for high methylation and low methylation of *PCDHA* gene family were set at 80% of the methylation index.
‡Boundaries for high methylation and low methylation of *HLP* were set at 10% of the methylation index.
§Boundaries for high methylation and low methylation of *CYP26C1* were set at 70% of the methylation index.
‖Boundaries for high methylation and low methylation of *DKFZp451I127* were set at 20% of the methylation index.

Effects of PCDHB Methylation on Gene Expression and Chromatin Structure. The CGIs of the *PCDHB* family were located in their gene bodies, whose methylation generally does not block gene transcription (17). The actual effects of methylation on expression were examined for 16 genes of the *PCDHB* family using 10 primary neuroblastomas with low methylation and five primary neuroblastomas with high methylation. The methylation was not associated with loss of expression (a representative result is shown in Fig. 4*A*). The effect of methylation of the *PCDHB16* CGI on the histone modification was further examined by chromatin immunoprecipitation assay. It was found that DNA methylation of the *PCDHB16* CGI did not induce histone H3 lysine 9 methylation or histone H3 deacetylation (data not shown).

Association between CIMP and Promoter Methylation. High methylation of *PCDHB* CGIs, a sensitive surrogate marker of CIMP in neuroblastomas, did not repress gene expression or induce histone modification. This indicated that CIMP is involved in the poor prognosis of neuroblastomas by causing methylation of promoter CGIs, although it is known that promoter CGIs are resistant to *de novo* methylation (18, 19).

Among the five CGI (groups) identified in this study, only that of *DKFZp451I127* was located in a promoter region. Although its methylation was infrequent, the methylation was observed only in neuroblastomas with CIMP (Table 1), and was associated with expression loss (Fig. 4*B*). To make the association clearer, methylation statuses were analyzed for eight additional CGIs in promoter regions. It was shown that methylation of promoter CGIs of *RASSF1A* (3p21) and *BLU* (3p21) was far more frequently observed in neuroblastomas with CIMP (Table 1, $P < 0.0001$). At the same time, there was a preference for CGIs affected by CIMP among CGIs in promoter regions, and also among those outside promoter regions (Table 2).

Discussion

Extensive methylation of multiple CGIs, conforming with the concept of CIMP, was here found specifically present in neuroblastomas with a poor prognosis and could be sensitively detected by focusing on the *PCDHB* family. *PCDHB* methylation did not suppress gene expression or induce histone modification. However, CIMP was associated with promoter methylation of *RASSF1A* and *BLU* genes and one of the mechanisms underlying the poor prognosis of neuroblastomas seemed to be silencing of these and possibly other tumor suppressor genes and genes important for differentiation.

CIMP was originally identified in colon cancers (16), but there has been some dispute over its presence (20). The clear correlation between CIMP and a poor prognosis found here for neuroblastomas was unequivocal and presumably reflects an intrinsic tendency for methylation of CGIs. This is because, first, neuroblastomas have a much shorter history than colon cancers, and the accumulated number of methylated CGIs in neuroblastomas is expected to parallel the speed of occurrence of

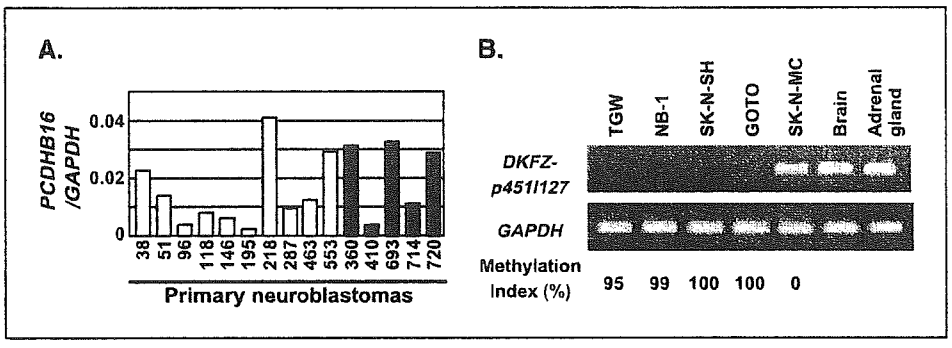

Figure 4. Effects of methylation of the *PCDHB* family and *DKFZp451I127* on gene expression. *A*, *PCDHB16* expression was analyzed by quantitative RT-PCR in 10 primary samples with low methylation (*open columns*) and five primary samples with high methylation (*closed columns*), and no difference was observed between the two groups. *B*, silencing of *DKFZp451I127* by methylation of its promoter CGI. The CGI was methylated in four cell lines, TGW, NB-1, SK-N-SH, and GOTO, whereas it was unmethylated in one cell line, SK-N-MC. *DKFZp451I127* was expressed in SK-N-MC, but not expressed at all in the four cell lines with the promoter methylation.

Table 2. HRs of death by *PCDHB* methylation status in subgroup of known prognostic factors

Stratified by		*PCDHB* methylation	No. cases	No. deaths	HR* (95% CI)	P†
Overall (n = 140)		High	67	1	22.1 (5.3-93.4)	< 0.0001
		Low	73	2	1	
N-*myc* amplification (n = 140)	No	High	30	8	12.4 (2.6-58.9)	0.002
		Low	72	2	1	
	Yes	High	37	20	NE	—
		Low	1	0		
TrkA overexpression (n = 130)	Yes	High	20	6	18.3 (2.2-152.6)	0.007
		Low	49	1	1	
	No	High	40	19	NE	
		Low	21	0		
DNA ploidy (n = 125)	Aneuploid	High	17	5	18.3 (2.1-156.7)	0.008
		Low	49	1	1	
	Diploid	High	38	17	NE	
		Low	21	0		
Clinical stages (n = 140)	Stages I, II, and IVS	High	8	0	NE	—
		Low	52	0		
	Stages III and IV	High	59	28	7.4 (1.8-31.3)	0.006
		Low	21	2	1	
Age at diagnosis (n = 140)	<1	High	11	3	NE	
	≥1	Low	59	0		
		High	56	25	4.5 (1.1-18.9)	0.043
		Low	14	2	1	

*HR of death for a case with high *PCDHB* methylation compared with a case with low methylation. NE shows not estimable due to no events in at least one category.
†Significance level for a high *PCDHB* methylation to low methylation using Cox proporitonal model.

methylation. Second, methylation of the *PCDHB* family did not affect gene expression, and there should have been no selection of cells with the *PCDHB* methylation, in contrast to the case of promoter methylation of tumor suppressor genes. Investigation into the mechanism of the intrinsic tendency for methylation of multiple CGIs is necessary. Furthermore, alleviation of the intrinsic tendency could block progression of neuroblastomas and have potential therapeutic value.

Among the six CGI (groups) outside promoter regions analyzed here, CIMP in neuroblastomas preferentially affected four CGI (groups); those of the *PCDHB* family, the *PCDHA* family, *HLP*, and *CYP26C1*. Unexpectedly, three CGIs that are known to be frequently methylated in human colon cancers with CIMP, MINT1, MINT2, and MINT17 (16) were not methylated in neuroblastoma cell lines (data not shown). Among the nine CGIs in promoter regions analyzed, CIMP in neuroblastomas affected only three, those of *RASSF1A*, *BLU*, and *DKFZp451I127*. The nine CGIs were selected based upon previous reports as tumor suppressor genes (*RASSF1A*, *BLU*, *p16*, and *hMLH1*; refs. 21–23), the chromosomal location flanking the *PCDHB* family (*PCDHB1* and *TAF7*), our previous report on the fidelity in inheriting methylation patterns (*p41Arc* and *SIM2*; ref. 19), and the findings here (*DKFZp451I127*). Because gene expression and possibly chromatin structures affect the frequency of *de novo* methylation (24, 25), the available data suggest that CGIs useful to sensitively detect CIMP might vary according to the tumor type.

The influence of CIMP on prognosis was here found to be comparable to that of the currently most reliable marker, N-*myc* amplification, and stronger than *TrkA* overexpression and DNA ploidy on univariate analysis. Subgroup analysis showed that the influence was independent of *TrkA* overexpression, DNA ploidy and age at diagnosis and CIMP had influence even in cases without N-*myc* amplification and in advanced stages. These points strongly indicated CIMP to be a promising new prognostic marker. However, the cutoff values adopted here are tentative, and the HRs obtained could have been overestimated. A validation study using independent samples is necessary for further evaluation. The fact that cases with CIMP contained almost all the cases with N-*myc* amplification suggested that a common molecular mechanism caused both alterations, or that CIMP may lead to N-*myc*

amplification. Whatever the case, the findings might provide clues to molecular mechanisms of neuroblastoma development.

In summary, the present study showed that CIMP is present specifically in neuroblastomas with poor prognosis and that can be sensitively detected by focusing on *PCDHB* methylation. CIMP seems to be a promising new prognostic marker, and its evaluation and investigations into the mechanisms underlying CIMP in neuroblastomas seem warranted.

Acknowledgments

Received 7/27/2004; revised 11/14/2004; accepted 11/24/2004.

Grant support: Grant-in-aid for the Third-term Cancer Control Strategy Program from the Ministry of Health, Labour, and Welfare, Japan and Research Resident Fellowship from the Foundation for Promotion of Cancer Research (M. Abe).

The costs of publication of this article were defrayed in part by the payment of page charges. This article must therefore be hereby marked advertisement in accordance with 18 U.S.C. Section 1734 solely to indicate this fact.

We thank Drs. E. Okochi-Takada and G. S. Goldberg for critical reading of the article and the institutions for participation in the collection of clinical materials.

References

1. Jones PA, Baylin SB. The fundamental role of epigenetic events in cancer. Nat Rev Genet 2002;3:415–28.
2. Chen RZ, Pettersson U, Beard C, Jackson-Grusby L, Jaenisch R. DNA hypomethylation leads to elevated mutation rates. Nature 1998;395:89–93.
3. Kondo Y, Kanai Y, Sakamoto M, et al. Genetic instability and aberrant DNA methylation in chronic hepatitis and cirrhosis-A comprehensive study of loss of heterozygosity and microsatellite instability at 39 loci and DNA hypermethylation on 8 CpG islands in microdissected specimens from patients with hepatocellular carcinoma. Hepatology 2000;32:970–9.
4. Ushijima T, Morimura K, Hosoya Y, et al. Establishment of methylation-sensitive-representational difference analysis and isolation of hypo- and hypermethylated genomic fragments in mouse liver tumors. Proc Natl Acad Sci U S A 1997;94:2284–9.
5. Kaneda A, Takai D, Kaminishi M, Okochi E, Ushijima T. Methylation-sensitive representational difference analysis and its application to cancer research. Ann N Y Acad Sci 2003;983:131–41.
6. Takai D, Yagi Y, Wakazono K, et al. Silencing of *HTR1B* and reduced expression of *EDN1* in human lung cancers, revealed by methylation-sensitive representational difference analysis. Oncogene 2001; 20:7505–13.
7. Kaneda A, Kaminishi M, Yanagihara K, Sugimura T, Ushijima T. Identification of silencing of nine genes in human gastric cancers. Cancer Res 2002;62:6645–50.
8. Miyamoto K, Asada K, Fukutomi T, et al. Methylation-associated silencing of heparan sulfate *D-glucosaminyl 3-O-sulfotransferase-2* (*3-OST-2*) in human breast, colon, lung and pancreatic cancers. Oncogene 2003;22:274–80.
9. Hagihara A, Miyamoto K, Furuta J, et al. Identification of 27 5′ CpG islands aberrantly methylated and 13 genes silenced in human pancreatic cancers. Oncogene 2004;23:8705–10.
10. Brodeur GM. Neuroblastoma: biological insights into a clinical enigma. Nat Rev. Cancer 2003;3:203–16.
11. Schwab M, Westermann F, Hero B, Berthold F. Neuroblastoma: biology and molecular and chromosomal pathology. Lancet Oncol 2003;4:472–80.
12. Nakagawara A, Arima-Nakagawara M, Scavarda NJ, et al. Association between high levels of expression of the *TRK* gene and favorable outcome in human neuroblastoma. N Engl J Med 1993;328:847–54.
13. Jaenisch R, Bird A. Epigenetic regulation of gene expression: how the genome integrates intrinsic and environmental signals. Nat Genet 2003;33:245–54.
14. Li E. Chromatin modification and epigenetic reprogramming in mammalian development. Nat Rev Genet 2002;3:662–73.
15. Kaneda A, Kaminishi M, Sugimura T, Ushijima T. Decreased expression of the seven ARP2/3 complex genes in human gastric cancers. Cancer Lett 2004; 212:203–10.
16. Toyota M, Ahuja N, Ohe-Toyota M, et al. CpG island methylator phenotype in colorectal cancer. Proc Natl Acad Sci U S A 1999;96:8681–6.
17. Gonzalgo ML, Hayashida T, Bender CM, et al. The role of DNA methylation in expression of the *p19/p16* locus in human bladder cancer cell lines. Cancer Res 1998;58:1245–52.
18. Nguyen C, Liang G, Nguyen TT, et al. Susceptibility of nonpromoter CpG islands to *de novo* methylation in normal and neoplastic cells. J Natl Cancer Inst 2001; 93:1465–72.
19. Ushijima T, Watanabe N, Okochi E, et al. Fidelity of the methylation pattern and its variation in the genome. Genome Res 2003;13:868–74.
20. Yamashita K, Dai T, Dai Y, Yamamoto F, Perucho M. Genetics supersedes epigenetics in colon cancer phenotype. Cancer Cell 2003;4:121–31.
21. Agathanggelou A, Dallol A, Zochbauer-Muller S, et al. Epigenetic inactivation of the candidate 3p21.3 suppressor gene *BLU* in human cancers. Oncogene 2003; 22:1580–8.
22. Takita J, Hayashi Y, Nakajima T, et al. The *p16* (*CDKN2A*) gene is involved in the growth of neuroblastoma cells and its expression is associated with prognosis of neuroblastoma patients. Oncogene 1998; 17:3137–43.
23. Harada K, Toyooka S, Maitra A, et al. Aberrant promoter methylation and silencing of the *RASSF1A* gene in pediatric tumors and cell lines. Oncogene 2002; 21:4345–9.
24. De Smet C, Loriot A, Boon T. Promoter-dependent mechanism leading to selective hypomethylation within the 5′ region of gene *MAGE-A1* in tumor cells. Mol Cell Biol 2004;24:4781–90.
25. Richards EJ, Elgin SC. Epigenetic codes for heterochromatin formation and silencing: rounding up the usual suspects. Cell 2002;108:489–500.

LMO3 Interacts with Neuronal Transcription Factor, HEN2, and Acts as an Oncogene in Neuroblastoma

Mineyoshi Aoyama,[1] Toshinori Ozaki,[1] Hiroyuki Inuzuka,[1] Daihachiro Tomotsune,[3] Junko Hirato,[4] Yoshiaki Okamoto,[1] Hisashi Tokita,[2] Miki Ohira,[1] and Akira Nakagawara[1]

Divisions of [1]Biochemistry and [2]Animal Science, Chiba Cancer Center Research Institute; [3]Center for Functional Genomics, Hisamitsu Pharmaceutical Co., Inc., Chiba, Japan and [4]Department of Pathology, Gunma University School of Medicine, Gunma, Japan

Abstract

LIM-only proteins (LMO), which consist of LMO1, LMO2, LMO3, and LMO4, are involved in cell fate determination and differentiation during embryonic development. Accumulating evidence suggests that LMO1 and LMO2 act as oncogenic proteins in T-cell acute lymphoblastic leukemia, whereas LMO4 has recently been implicated in the genesis of breast cancer. However, little is known about the role of LMO3 in either tumorigenesis or development. In the present study, we have identified *LMO3* and *HEN2*, which encodes a neuronal basic helix-loop-helix protein, as genes whose expression levels were higher in unfavorable neuroblastomas compared with those of favorable tumors. Immunoprecipitation and immunostaining experiments showed that LMO3 was associated with HEN2 in mammalian cell nucleus. Human neuroblastoma SH-SY5Y cells stably overexpressing LMO3 showed a marked increase in cell growth, a promotion of colony formation in soft agar medium, and a rapid tumor growth in nude mice compared with the control transfectants. More importantly, the increased expression of LMO3 and HEN2 was significantly associated with a poor prognosis in 87 primary neuroblastomas. These results suggest that the deregulated expression of neuronal-specific LMO3 and HEN2 contributes to the genesis and progression of human neuroblastoma in a lineage-specific manner. (Cancer Res 2005; 65(11): 4587-97)

Introduction

The LIM domain–containing proteins are important regulators in determining cell fate and controlling cell growth and differentiation during embryonic development (1). The LIM domain is a highly conserved cysteine-rich zinc finger–like motif found in a variety of nuclear and cytoplasmic proteins and acts as a docking site for the assembly of multiprotein complexes (2–4). However, the precise role of the LIM domain is still unclear. Several distinct subgroups of the LIM domain–containing proteins are defined and some of them also possess a functionally divergent domain, including a DNA-binding homeodomain or a protein kinase domain (1, 2).

The LIM-only proteins (LMO) are one of the families of the LIM domain–containing proteins and possess only two tandem LIM domains. They consist of four members, including LMO1, LMO2, LMO3, and LMO4 (2, 4). *LMO1* and *LMO2* have been identified as the genes that are activated in human acute T-cell leukemia (T-cell ALL) by tumor-specific chromosomal translocations (4). Transgenic mice overexpressing LMO1 or LMO2 developed immature and aggressive T-cell leukemia, suggesting that these proteins act as T-cell oncoproteins (5–7). On the other hand, LMO4 has been identified as a nuclear protein that interacts with the adaptor protein Ldb1 (8). It has been shown recently that LMO4 is highly expressed in primary human breast cancers, and overexpression of LMO4 inhibits differentiation of mammary epithelial cells, suggesting that deregulated expression of LMO4 contributes to the breast carcinogenesis (9). LMO4 has also been reported to be associated with BRCA1 to repress its transcriptional activity (10). Thus, LMO1, LMO2, and LMO4 have been implicated in tumorigenesis. However, to date, little is known about the oncogenic function of LMO3, which has been discovered based on sequence homology with LMO1 (11).

The nuclear LMO proteins, which lack intrinsic DNA-binding activity, have been considered to be involved in transcriptional regulation (2), raising a possibility that they alter the transcription of target genes by forming a complex with other transcription factors with DNA-binding activity. Indeed, in T-cell acute lymphoblastic leukemia in children, a basic helix-loop-helix transcription factor, TAL1, is physically associated with LMO1 or LMO2 and enhances their oncogenic activities (12, 13). Interestingly, the neuronal-specific basic helix-loop-helix transcription factors, HEN1 and HEN2, were identified based on cross-hybridization with TAL1 (14, 15). Their expression was restricted to the developing nervous system and a human neuroblastoma cell line. However, the role of HEN1 and HEN2 in tumorigenesis has long been elusive.

Neuroblastoma is one of the most common childhood cancers and is originated from sympathoadrenal lineage of the neural crest (16). It is clinically and cytogenetically divided into two major subgroups with favorable and unfavorable prognosis (17). The recent molecular and cellular analyses have revealed that amplification of *MYCN* and *DDX1* as well as loss of heterozygosity at the region of chromosome 1p36 are strongly associated with a poor outcome, whereas high levels of expression of the neurotrophin receptors *TrkA*, *CD44*, and *Fyn*, are well correlated with favorable prognosis (16–23). However, we still do not know many other genes that play important roles in the genesis and progression of neuroblastoma. To identify the other genes closely involved in neuroblastoma, we have constructed several cDNA libraries from different subsets of neuroblastoma and randomly cloned 4,200 genes (24). Screening of the genes differentially expressed between favorable and unfavorable subsets of the tumor has identified *Nbla3267* as one of the genes expressed at higher levels in unfavorable than favorable neuroblastomas (25).

In the present study, we found that *Nbla3267* encoded the human LMO, LMO3, and that high expression of *LMO3* as well as *HEN2* was strongly associated with a poor prognosis of neuroblastoma. Furthermore, LMO3 interacted with HEN2 in mammalian

Requests for reprints: Akira Nakagawara, Division of Biochemistry, Chiba Cancer Center Research Institute, 666-2 Nitona, Chuoh-ku, Chiba 260-8717, Japan. Phone: 81-43-264-5431; Fax: 81-43-265-4459; E-mail: akiranak@chiba-cc.jp.

cell nucleus, and enforced expression of LMO3 in human neuroblastoma-derived cell line SH-SY5Y markedly enhanced tumor growth in nude mice, supporting the oncogenic role of LMO3 in neuroblastoma.

Materials and Methods

Patient population. The RNA samples obtained from 87 patients with neuroblastoma were subjected to semiquantitative and quantitative real-time reverse transcription-PCR (RT-PCR) analyses. All patients were diagnosed clinically as well as pathologically and tested for DNA ploidy, MYCN amplification, and TrkA expression. Tumors were staged according to the International Neuroblastoma Staging System criteria (26). Thirty-four patients were stage I, 14 were stage II, 8 were stage III, 26 were stage IV, and 5 were stage IVS. Stages I, II, and IVS were considered as favorable and stages III and IV as unfavorable. The patients were treated following the protocols proposed by the Japanese Infantile Neuroblastoma Cooperative Study (27) and the Study Group of Japan for Treatment of Advanced Neuroblastoma (28). The clinical follow-up ranged from 4 to 58 months, with a median of 36 months. We have a precise list of patient characteristics, including age, stage, and clinical follow-up time, and this list will be provided upon request.

Cloning of human *LMO3*, *HEN1*, and *HEN2*. To obtain a complete human *LMO3* cDNA, a cDNA library derived from human fetal brain (Stratagene, La Jolla, CA) was screened with a ^{32}P-labeled *Nbla3267* cDNA. Plaques showing positive signals were picked up and rescreened twice. To construct the expression plasmid for hemagglutinin (HA)–tagged LMO3-A, the cDNA fragment encoding the entire LMO3-A protein was amplified by PCR from the phage clone as a template using the primers designed to add a synthetic linker encoding the HA epitope on the NH_2-terminal side of LMO3-A (forward 5′-GGTACCATGGCTTACCCATACGATGTTCCAGATTACGCTAGCCTCTCAGTCCAGCCAGACAC-3′ and reverse 5′-TCAGATATCATTAGATCAGCGAACCTGGG-3′). The PCR product was digested with *Kpn*I and *Eco*RV and subcloned into the identical restriction sites of pcDNA3 expression plasmid to give pcDNA3-HA-LMO3-A. cDNA encoding human HEN1 (amino acid residues 1-133) or HEN2 (amino acid residues 1-135) was generated by reverse transcribing total RNA isolated from neuroblastoma cell line, IMR32, using a forward primer (5′-AAGGAATTCATGCTCAACTCAGACACCATG-3′) and a reverse primer (5′-ATAAGAATGCGGCCGCTCAGACGT-3′) for HEN1 and a forward primer (5′-AAGGAATTCATGCTGAGTCCGGACCAAGCA-3′) and a reverse primer (5′-ATAAGAATGCGGCCGCCTACACGTCCAGGACGTGGTT-3′) for HEN2. The amplified PCR products were digested with *Eco*RI and *Not*I and subcloned into the identical restriction sites of pcDNA3-FLAG expression plasmid to give pcDNA-FLAG-HEN1 and pcDNA3-FLAG-HEN2.

Generation of a polyclonal anti-LMO3 antibody. The polyclonal anti-LMO3 and anti-HEN2 antibodies were raised against a peptide "Cys" plus containing the amino acid sequence between positions 127 and 145 of LMO3 and the amino acid sequence between positions 1 and 19 of HEN2, respectively. The peptides and the polyclonal antibodies were produced by Biologica Co. (Nagoya, Japan).

Cell culture and transfection. Human neuroblastoma (SK-N-AS, SH-SY5Y, NB69, OAN, SK-N-BE, NGP, NLF, IMR32, NB1, and KP-N-NS), ALL (RPMI, KOPT, HSB, and MOLT), osteosarcoma (OST, SAOS-2, and U2OS), rhabdomyosarcoma (RMS-MK), colon cancer (COLO-320), breast cancer (MCF-7 and MDA-MB-453), melanoma (G361, G32TG, and A875), thyroid cancer (TTC11), small cell lung carcinoma (H1299), and cervical cancer (HeLa) cell lines and COS7 cells were maintained in RPMI 1640 or DMEM supplemented with 10% heat-inactivated fetal bovine serum (FBS), 100 IU/mL penicillin, and 100 μg/mL streptomycin at 37°C in an atmosphere of 5% CO_2 in the air. For transient transfection, COS7 cells were transfected with the indicated expression plasmids using FuGene 6 transfection reagent as recommended by the manufacturer (Roche Molecular Biochemicals, Mannheim, Germany). Stable transfections of SH-SY5Y cells were done with the empty plasmid (pcDNA3, Invitrogen, Carlsbad, CA) or with the expression plasmid for FLAG-tagged LMO3-A using Lipofect-AMINE Plus transfection reagent according to the manufacturer's instructions (Invitrogen). The transfected cells were cultured in the presence of G418 at a final concentration of 400 μg/mL (Sigma Chemical Co., St. Louis, MO). Thereafter, the selection medium was replaced every 3 days. Three weeks after the selection in G418, drug-resistant clones were isolated and allowed to proliferate in medium containing G418.

Reverse transcription-PCR analysis. Total RNA was prepared from cultured cells and human tissues by using Trizol reagent (Life Technologies, Grand Island, NY) or the RNeasy Mini kit (Qiagen, Valencia, CA). Reverse transcription was carried out using random primers and SuperScript II (Invitrogen). Following the reverse transcription, the resultant cDNA was subjected to PCR-based amplification. Oligonucleotides used to amplify *LMO3-A*, *LMO3-B*, *LMO1*, *LMO2*, *LMO4*, *Ldb1*, *Ldb2*, *TAL1*, *HEN1*, *HEN2*, and glyceraldehyde-3-phosphate dehydrogenase (*GAPDH*) mRNAs were as follows: *LMO3-A*: forward 5′-ACTGTGCTTACTGAACGGCCTC-3′ and reverse 5′-CCGGTCCTTGATCTTTCGGTTG-3′; *LMO3-B*: forward 5′-TGCAACTCAGACACGCCTAAG-3′ and reverse 5′-CCGGTCCTTGATCTTTCGGTTG-3′; *LMO1*: forward 5′-GCTCCACCCTCTACACCAAG-3′ and reverse 5′-CTGCCCTTCCTCATAGTCCA-3′; *LMO2*: forward 5′-AATGCGGGTGAAAGACAAAG-3′ and reverse 5′-CCCCAAAGTGCCTAAGAGTG-3′; *LMO4*: forward 5′-GCAAGGCAATGTGTATCATCT-3′ and reverse 5′-GCATTCTGCATTACTCTGACC-3′; *Ldb1*: forward 5′-CCAGGGAGCAGAAGACAGAA-3′ and reverse 5′-AGAGGCCCAGGTTCCAAG-3′; *Ldb2*: forward 5′-TAGCCCAAGTGCTGAAACAA-3′ and reverse 5′-TAAACTGCCCACAAAACCAA-3′; *TAL1*: forward 5′-GTTCTTAGGCTGCTGGGATG-3′ and reverse 5′-GATTTGGGACTGAGGGAAGA-3′; *HEN1*: forward 5′-AGAGACTGAGTCGGGCTTCA-3′ and reverse 5′-CAGGCGCAGAATCTCAATCT-3′; *HEN2*: forward 5′-CCCCAAGGGTTGTGGTTTTA-3′ and reverse 5′-TCTGAACTTCTGCCCTCATTCTTT-3′; and *GAPDH*: forward 5′-ACCTGACCTGCCGTCTAGAA-3′ and reverse 5′-TCCACCACCCTGTTGCTGTA-3′. Amplified products were electrophoretically separated on agarose gels and visualized by ethidium bromide staining. The gels were photographed under UV illumination.

Northern analysis. A human MTN blot (Clontech, Palo Alto, CA), a nylon membrane on which poly(A)$^+$ RNAs extracted from various human normal tissues were blotted, was used for analysis of the distribution of *LMO3* expression in human normal tissues. ^{32}P-labeled probe was prepared by random priming of the 2.5-kb restriction fragment of *LMO3* cDNA. The membrane was hybridized overnight at 65°C in a solution containing 7.5% dextran sulfate, 1 mol/L NaCl, 1% *N*-lauroyl sarcosine, 100 μg/mL heat-denatured salmon sperm DNA, and the radiolabeled probe. The membrane was washed twice in 0.5 × SSC/0.1% *N*-lauroyl sarcosine at 50°C. Specific signals were obtained by autoradiography.

Section *in situ* hybridization. Section *in situ* hybridization was done as described previously (29). A riboprobe was synthesized with digoxygenin-UTP and T3 or T7 polymerase (Roche Molecular Biochemicals). The alkaline phosphatase reaction was done with nitroblue tetrazolium/5-bromo-4-chloro-3-indolyl phosphate (Roche Molecular Biochemicals). The riboprobe used for the section *in situ* hybridization were transcripts of the human cDNA fragments of the *LMO3* gene.

Immunohistochemistry. Neuroblastoma tissues were stained with immunoperoxidase method using anti-HEN2 antibody. They included unfavorable neuroblastomas with *MYCN* gene amplification and favorable neuroblastomas with a single copy of *MYCN* gene. Neuroblastoma specimens were fixed in 10% buffered formalin and embedded in paraffin, and 3 μm sections were applied to the immunostaining. Before incubation with anti-HEN2 antibody, the sections were treated with 0.05% Pronase in 0.05 mol/L Tris-HCl (pH 7.6) for 5 minutes. The sections were incubated with anti-HEN2 antibody, which was diluted to 1:200 at 4°C overnight. The biotin-streptavidin method (Nichirei, Tokyo, Japan) was done, and the sections were visualized with diaminobenzidine solution. The nuclei were counterstained with hematoxylin.

Immunofluorescent staining. COS7 cells were doubly transfected with the expression plasmids for HA-LMO3-A and FLAG-HEN2. Forty-eight hours after transfection, cells were fixed for 30 minutes with 3.7% formaldehyde in PBS and permeabilized with 0.2% Triton X-100 for 5 minutes, and nonspecific epitopes were blocked for 1 hour in PBS containing 3% bovine serum albumin. The cells were then incubated with a polyclonal anti-HA antibody (1:200 dilution, Medical and Biological Laboratories, Nagoya,

Japan) and a monoclonal anti-FLAG antibody (1:50, M2, Sigma Chemical). After three washes with PBS, cells were stained with a FITC- or a rhodamine-conjugated secondary antibody (1:200, Invitrogen). The coverslips were mounted onto glass slides, and the stained cells were viewed using a confocal laser scanning microscope (Olympus, Tokyo, Japan).

Western blot analysis and immunoprecipitation. After transfection, cells were rinsed twice with ice-cold PBS and then lysed immediately with SDS sample buffer. Equal amounts of proteins were separated under denaturing conditions by electrophoresis in 15% polyacrylamide gel containing SDS-PAGE and electrotransferred to polyvinylidene difluoride membrane (Immobilon-P, Millipore, Bedford, MA). After blocking in a solution containing 5% skim milk, the membrane was incubated with a monoclonal anti-FLAG, a polyclonal anti-HA, a polyclonal anti-LMO3, or a polyclonal anti-actin antibody (20-33, Sigma Chemical) and then incubated with a horseradish peroxidase–conjugated goat anti-mouse or anti-rabbit secondary antibody (Jackson ImmunoResearch Laboratories, West Grove, PA). Protein bands were visualized with an enhanced chemiluminescence (Amersham Pharmacia Biotech, Piscataway, NJ). For immunoprecipitation, transfected cells were lysed in EBC buffer [50 mmol/L Tris-HCl (pH 7.5), 120 mmol/L NaCl, 0.5% NP40, 1 mmol/L phenylmethylsulfonyl fluoride] containing protease inhibitor mixture (Sigma Chemical). The precleared soluble supernatants were mixed with a polyclonal anti-HA or a monoclonal anti-FLAG antibody and incubated for 2 hours at 4°C. Protein A-Sepharose beads were then added to the reaction mixtures and incubated for 1 hour at 4°C. The immune complexes were washed with the lysis buffer thrice at 4°C. The bound proteins were resuspended in SDS sample buffer, resolved by SDS-PAGE, and analyzed by Western blotting.

Cell proliferation and soft agar assay. Cells were seeded in triplicate in 24-well plates (5×10^3 per well) in culture medium containing 10% or 1% FBS. Cells were allowed to adhere to the bottom of the cell culture dish for 24 hours. At the indicated times, cells were trypsinized and cell counting was carried out using a Coulter Counter (Coulter Electronics Ltd., Hialeah, Finland). For soft agar assay, 2.5×10^3 cells of the stable transfectants or the parental SH-SY5Y cells were seeded in triplicate in 35-mm cell culture plates containing 0.2% agar and RPMI 1640 supplemented with 10% FBS. After 21 days, colonies with diameters >300 μm were scored as positive.

Tumor formation in nude mice. For tumor formation, 6-week-old female athymic *nu/nu* mice (Charles River Laboratory, Sulzfeld, Germany) were injected into the femur with 5×10^6 parental SH-SY5Y cells or SH-SY5Y cells transfected with the empty plasmid or with the expression plasmid encoding LMO3-A suspended in 100 μL PBS. Tumor size and body weight were measured once weekly and mice were sacrificed 7 weeks after injection. For histologic examinations, tumor tissues were fixed in fresh 10% buffered formalin and embedded in paraffin. The handling of animals was in accordance with the guidelines of the Chiba Cancer Center Research Institute (Chiba, Japan).

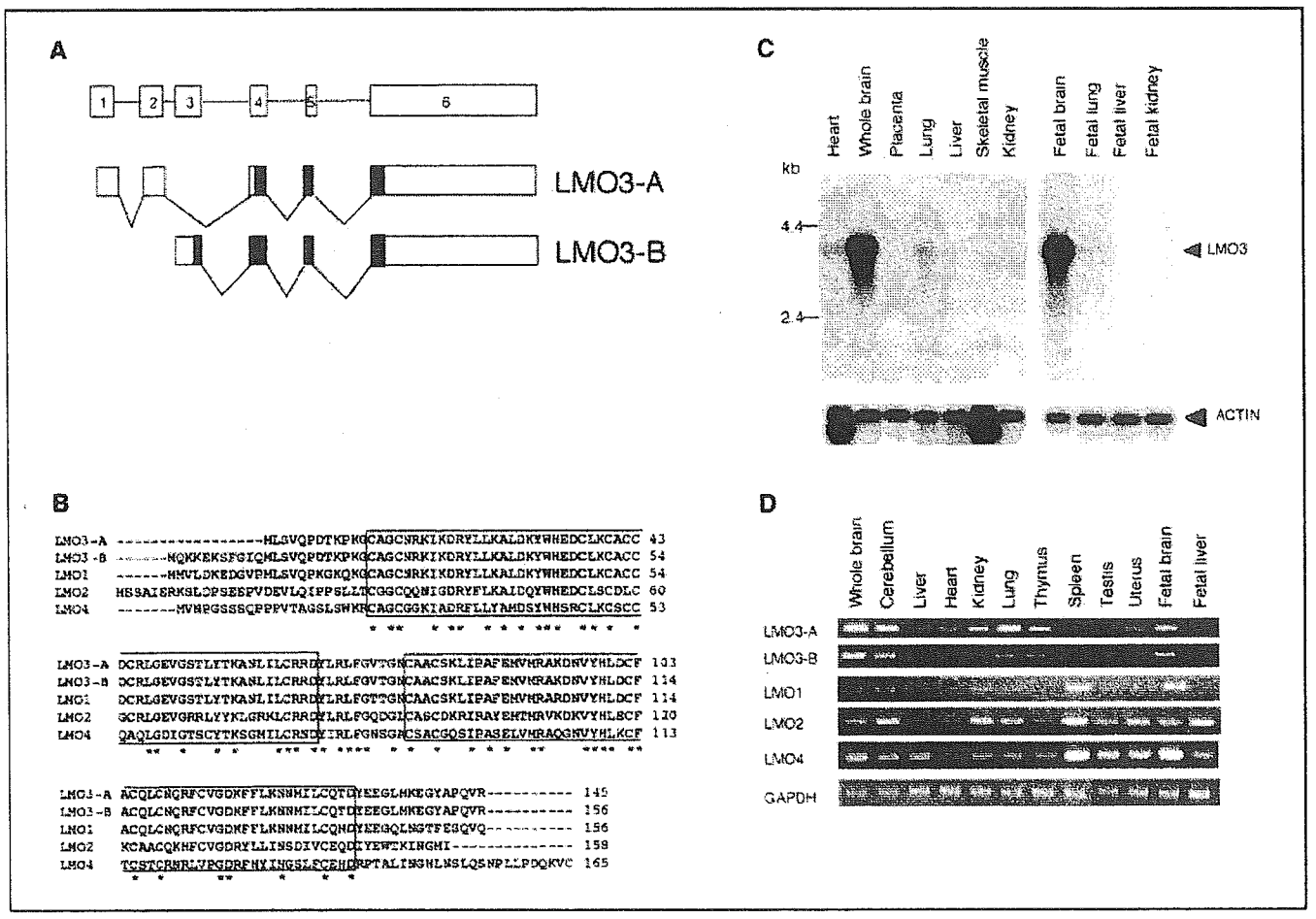

Figure 1. Identification of human LMO3-A and LMO3-B and their relation to the other LMO family members. *A*, schematic representation of the exons of human *LMO3* gene. *Solid* and *open boxes*, coding and untranslated regions, respectively. *B*, deduced amino acid sequences of human LMO3-A and LMO3-B and their alignments with those of human LMO1, LMO2, and LMO4. *Asterisks*, identical amino acid residues. Two LIM domains are *boxed*. *C*, tissue-specific expression of *LMO3*. Human multiple tissue Northern blots containing poly(A)$^+$ RNA were hybridized with a radiolabeled human *LMO3* cDNA (*top*) or with a radioactive probe derived from human *β-actin* cDNA (*bottom*). β-actin was used as a control for equal loading. The 2-kb band was hybridized ubiquitously, and an additional 1.8-kb band was hybridized in heart and skeletal muscle with the β-actin probe. *D*, coordinated expression of *LMO3-A* and *LMO3-B* in various human tissues. Total RNA isolated from the indicated human tissues was subjected to RT-PCR analysis to examine the expression levels of *LMO3-A*, *LMO3-B*, *LMO1*, *LMO2*, and *LMO4*. *GAPDH* expression is shown as an internal control.

Quantitative real-time PCR. Total RNA prepared from primary neuroblastomas was reverse transcribed into cDNA (SuperScript II kit) and subjected to the real-time PCR. The expression level of *GAPDH* was measured in all samples to normalize *LMO3* and *HEN2* expression according to the manufacturer's instructions (Applied Biosystems, Foster City, CA). Oligonucleotide primers and TaqMan probes, which were labeled at the 5′ end with the reporter dye 6-carboxyfluorescein (FAM) and at the 3′ end with the quencher dye 6-carboxytetramethylrhodamine (TAMRA), were as follows: *LMO3*: forward 5′-TCTGAGGCTCTT-TGGTGTAACG-3′, reverse 5′-CCAGGTGGTAAACATTGTCCTTG-3′, and probe 5′-FAM-AAACTGCGCTGCCTGTAGTAAGCTCATCC-TAMRA-3′ and *HEN2*: forward 5′-CCCCAAGGGTTGTGGTTTTA-3′, reverse 5′-TCTGAACTTCTGCCCTCATTCTTT-3′, and probe 5′-FAM-TTGAGTTCTCC-TACATTCATCCGCCACAA-TAMRA-3′. Amplification and detection were done using the ABI Prism 7700 Sequence Detection System (Applied Biosystems).

Statistical analysis. Student's *t* tests were used to explore possible associations between *LMO3* expression and other factors. Because the values of the *LMO3* expression were skewed, a log transformation was used to achieve the normality in the analyses using *t* test and Cox regression. The distinction between high and low levels of *LMO3* expression was based on the median value (low, *LMO3* < 0.2493 e.u.; high, *LMO3* > 0.2493 e.u.) regardless of tumor stage, *MYCN* copy number, or survival. The distinction between high and low levels of *HEN2* expression was based on the distribution of the values (low, undetectable; high, detectable). χ^2 tests were used to examine possible associations between *HEN2* expression and other factors, such as tumor stage. Kaplan-Meier survival curves were calculated, and survival distributions were compared using the log-rank test. Cox regression models were used to explore associations among *LMO3* expression, *HEN2* expression, age, *MYCN* amplification, mass screening, origin, and survival. Statistical significance was declared if $P < 0.05$. The statistical analysis was done using Stata Statistical Software Release 7.0 (Stata Corp., College Station, TX, 2001).

Results

Identification of the human *LMO3* gene. To identify the genes specifically involved in the genesis and progression of neuroblastoma, we have previously constructed cDNA libraries from the primary neuroblastomas and screened for the differentially expressed genes between the tumors with good and poor clinical outcome (25). One of the cDNA clones, *Nbla3267*, significantly overexpressed in the poor prognostic neuroblastomas contained a partial nucleotide sequence encoding a LMO family protein, LMO3. To obtain the missing 5′ part of the *LMO3* cDNA, we screened a cDNA library derived from human fetal brain. From ~6 × 10^5 recombinant phage clones, 10 independent phage clones were isolated. Sequence analysis

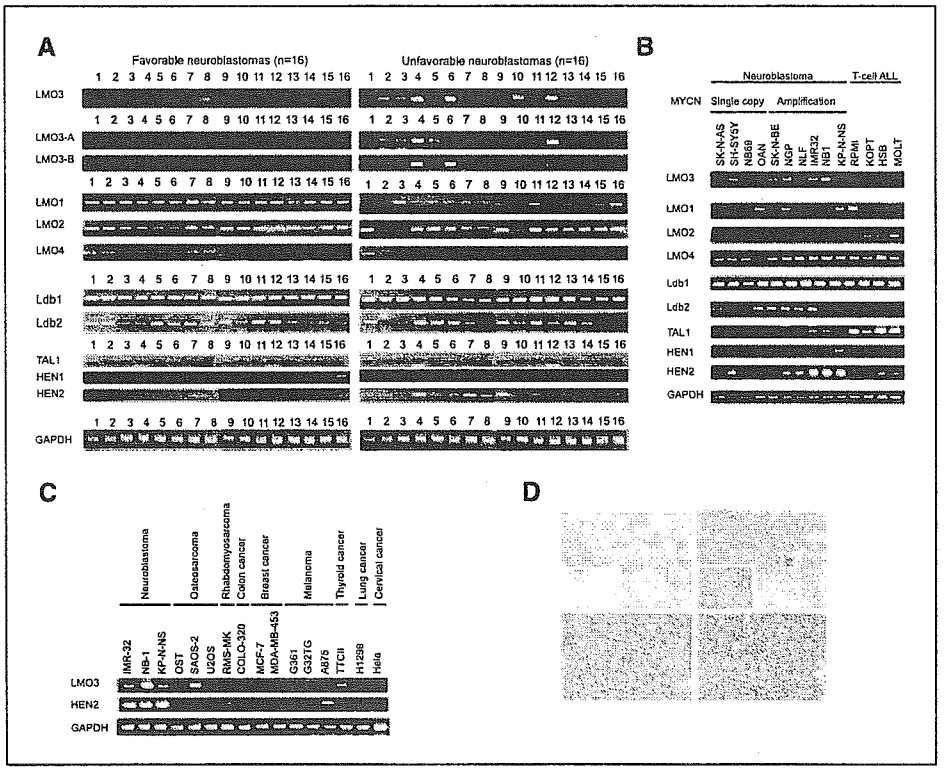

Figure 2. Increased expression of *LMO3* and *HEN2* in unfavorable neuroblastomas and neuroblastoma-derived cell lines. *A*, expression of *LMO3* and *LMO*-related genes in primary neuroblastomas with favorable (stage I, a single copy of *MYCN* and high expression of *TrkA*) and unfavorable (stages III and IV, *MYCN* amplification and decreased expression of *TrkA*) characteristics. Total RNA was isolated from the indicated neuroblastoma tissues, reverse transcribed, and amplified by PCR to examine the expression levels of *LMO3*, *LMO3-A*, *LMO3-B*, *LMO1*, *LMO2*, *LMO4*, *Ldb1*, *Ldb2*, *TAL1*, *HEN1*, and *HEN2*. Expression of *GAPDH* serves as an internal control. PCR products were visualized by ethidium bromide staining. *B*, expression of *LMO3* and *LMO*-related genes in neuroblastoma cell lines without *MYCN* amplification (SK-N-AS, SH-SY5Y, NB69, and OAN), neuroblastoma cell lines with *MYCN* amplification (SK-N-BE, NGP, NLF, IMR32, NB1, and KP-N-NS), and ALL cell lines (RPMI, KOPT, HSB, and MOLT). Total RNA prepared from the indicated cultured cells was subjected to RT-PCR analysis. Expression of *GAPDH* serves as an internal control. *C*, expression of *LMO3* and *HEN2* in various tumor-derived cell lines. Total RNA prepared from the indicated culture cells was subjected to RT-PCR analysis as described above. *D*, section *in situ* hybridization of neuroblastoma with the *LMO3* probe. Serial sections of the favorable neuroblastoma tissue (*top left* and *inset*) or the unfavorable one with *MYCN* amplification (*top right* and *inset*) were prepared, and expression of the *LMO3* gene was examined by section *in situ* hybridization. The *LMO3* transcripts are positive in unfavorable neuroblastoma. Immunohistochemical staining of HEN2 in primary neuroblastoma tissues. HEN2 is strongly positive in the nucleus of most tumor cells with *MYCN* amplification (*bottom right*), whereas it is negative in the favorable neuroblastoma tissue (*bottom left*).

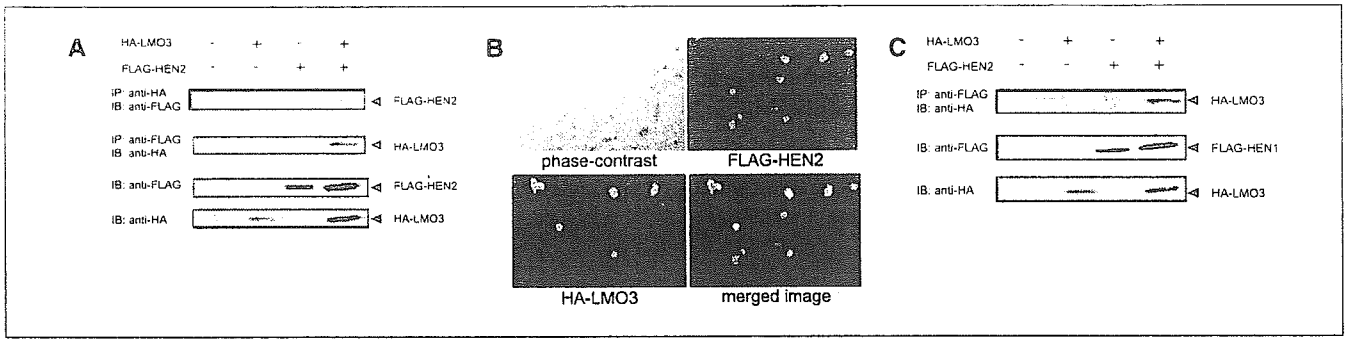

Figure 3. LMO3 interacts with HEN2 in mammalian cells. *A*, coimmunoprecipitation analysis. COS7 cells were transfected with the indicated expression plasmids. Forty-eight hours after transfection, whole cell lysates were prepared and subjected to the immunoprecipitation/Western analysis (*top* and *top middle*). Whole cell lysates were monitored on immunoblot for the expression of FLAG-HEN2 (*bottom middle*) and HA-LMO3-A (*bottom*). *B*, nuclear colocalization of LMO3 and HEN2 in cultured cells. COS7 cells were cotransfected with the expression plasmids for HA-LMO3-A and FLAG-HEN2. Forty-eight hours after transfection, cells were fixed and incubated with the polyclonal anti-HA and monoclonal anti-FLAG antibodies. Cells were then processed for double immunofluorescence using the FITC-conjugated anti-rabbit IgG (*green*) and with the rhodamine-conjugated anti-mouse IgG (*red*). The merged images (*yellow*) suggest the nuclear colocalization of LMO3 and HEN2. The phase-contrast images are also shown. *C*, coimmunoprecipitation of FLAG-HEN1 and HA-LMO3. Whole cell lysates prepared from COS7 cells transfected with the indicated combinations of the expression plasmids were immunoprecipitated with the anti-FLAG antibody followed by immunoblotting with the anti-HA antibody (*top*). Levels of FLAG-HEN1 and HA-LMO3 were also examined by immunoblotting with the anti-FLAG antibody (*middle*) and with the anti-HA antibody (*bottom*), respectively.

revealed that they were divided into two types, designated LMO3-A (145 amino acids) and LMO3-B (156 amino acids), with the different translation initiation sites. The NH_2-terminal region of LMO3-A was identical to that of the previously reported LMO3 protein (11). As shown in Fig. 1*A*, the putative translation initiation sites of LMO3-A and LMO3-B were located within exons 4 and 3, respectively. Because *LMO3* is a single gene, it is likely that LMO3-A and LMO3-B arise from differential splicing

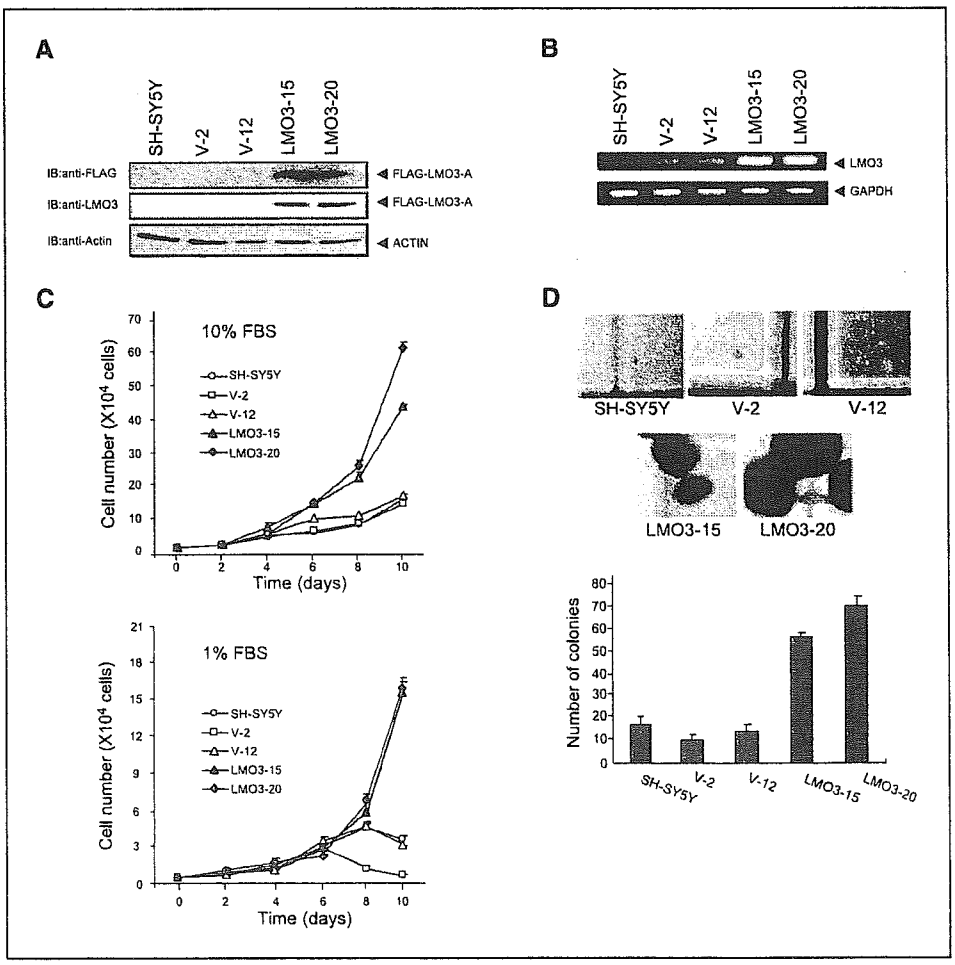

Figure 4. Growth-promoting activity of LMO3 in SH-SY5Y cells. *A*, stable SH-SY5Y transfectants expressing exogenous FLAG-LMO3-A. SH-SY5Y cells were stably transfected with the empty plasmid or with the expression plasmid for FLAG-LMO3-A and maintained in the presence of G418 (at a final concentration of 400 μg/mL) for 3 weeks. Whole cell lysates prepared from the indicated drug-resistant cell clones in addition to the parental SH-SY5Y cells were subjected to Western blot analysis using the anti-FLAG (*top*), anti-LMO3 (*middle*), or anti-actin (*bottom*) antibody. *B*, RT-PCR analysis of LMO3 in the indicated stable transfectants along with the parental SH-SY5Y cells. Expression of GAPDH serves as an internal control. *C*, effects of LMO3 overexpression on cell growth in SH-SY5Y cells. SH-SY5Y cells and the indicated transfectants were grown in the culture medium containing 10% (*top*) or 1% (*bottom*) FBS. Cells were harvested at 48-hour time intervals and number of cells was counted in triplicate. *Points*, means from three independent experiments; *bars*, SE. *D*, anchorage-independent growth of LMO3-overexpressing transfectants. The parental SH-SY5Y cells and the indicated transfectants (2.5×10^3 cells per dish) were grown in soft agar medium. After 3 weeks of culture, cells were examined by phase-contrast microscopy (*top*), and the numbers of colonies with a diameter of >300 μm were counted (*bottom*). *Columns*, means from three independent experiments; *bars*, SE.

or alternative promoter usage. Amino acid sequence alignment of LMO3 with the other LMO family proteins (LMO1, LMO2, and LMO4) showed a significant homology among them (Fig. 1*B*). LIM domains of LMO3 presented 98%, 60%, and 55% amino acid homology with those of LMO1, LMO2, and LMO4, respectively.

To determine the expression pattern of human *LMO3* mRNA, we did Northern blot analysis on a human multiple tissues blot using β-actin as a control. As shown in Fig. 1*C*, *LMO3* mRNA (~4 kb) was abundantly expressed in brain and at relatively low levels in the heart and lung but not in the other tissues examined. Similar to the adult tissues, *LMO3* mRNA was expressed predominantly in fetal brain, with a lower level in fetal lung. We then compared the tissue distribution of *LMO3-A* expression with those of *LMO3-B* and the other *LMO* family gene expression in various human adult and fetal tissues by RT-PCR (Fig. 1*D*). The expression pattern of *LMO3-A* was similar to that of *LMO3-B*, with relatively higher levels in brain, cerebellum, and fetal brain. In contrast, *LMO2* and *LMO4* were expressed ubiquitously in human tissues, and *LMO1* was expressed at higher levels in spleen and fetal brain.

Expression of *LMO3* and *HEN2* in aggressive neuroblastomas. As described previously, LMO family protein interacts with the nuclear LIM domain–binding protein 1 and 2 (Ldb1 and Ldb2), which act as adaptors for several LIM domain–containing proteins (30–32), and also binds to the basic helix-loop-helix transcription factor, TAL1, to regulate its transcriptional activity (12, 33, 34). Of interest, HEN1 and HEN2 were previously identified based on their homology with TAL1, and it was shown that LMO3 was associated with HEN1 (35). Furthermore, TAL1 was coexpressed with LMO1 or LMO2 in T-cell ALL (36), and double transgenic mice overexpressing TAL1 and LMO1 or LMO2 developed leukemia (37). As shown in Fig. 2*A*, *LMO3* (A and B) and *HEN2* were expressed at higher levels in unfavorable neuroblastomas compared with favorable tumors, whereas the levels of *LMO1* expression were predominantly high in the favorable tumors. No significant changes in the expression levels of *LMO2*, *Ldb1*, and *Ldb2* were detected between unfavorable and favorable neuroblastomas. *LMO4*, *TAL1*, and *HEN1* showed extremely low levels of expression in both types of neuroblastoma. We then studied the expression of these genes in 10 neuroblastoma and 4 T-cell ALL cell lines to examine the presence or absence of the lineage specificity, neuronal or hematopoietic. Consistent with the previous reports (36), *LMO2* and *TAL1* were coexpressed in T-cell ALL-derived cell lines (RPMI, KOPT, HSB, and MOLT; Fig. 2*B*). However, of interest, *LMO3* and *Ldb2* were expressed predominantly in neuroblastoma cell lines compared with the leukemia-derived lines. In addition, *HEN2* tended to be less highly expressed in leukemia cells compared with neuroblastoma cells. *HEN1* expression was also restricted to neuroblastoma but limited to only a few cell lines. On the other hand, there was no difference in the expression of *LMO4* and *Ldb1* between neuroblastoma-derived and T-cell ALL-derived cell lines. Interestingly, coexpression of *LMO3* and *HEN2* was observed in the majority of neuroblastoma cell lines but not in the other tumor-derived cell lines with different origin (Fig. 2*C*). These results revealed that only *LMO3* and *HEN2* were expressed at high levels in aggressive neuroblastomas in a neuronal-specific pattern.

Figure 2*D* shows the results of *in situ* hybridization for *LMO3* in primary neuroblastomas. *LMO3* mRNA was expressed in a stage IV neuroblastoma with *MYCN* amplification, whereas it was negative in a stage I tumor with a single copy of *MYCN* and high expression of *TrkA*. Unfortunately, our antibody raised against human LMO3 protein did not work for the immunohistochemical analysis. The immunostaining of HEN2 was also strongly positive in the nuclei of most tumor cells in *MYCN*-amplified neuroblastoma, albeit it was negative in favorable subset of the tumor (Fig. 2*D*).

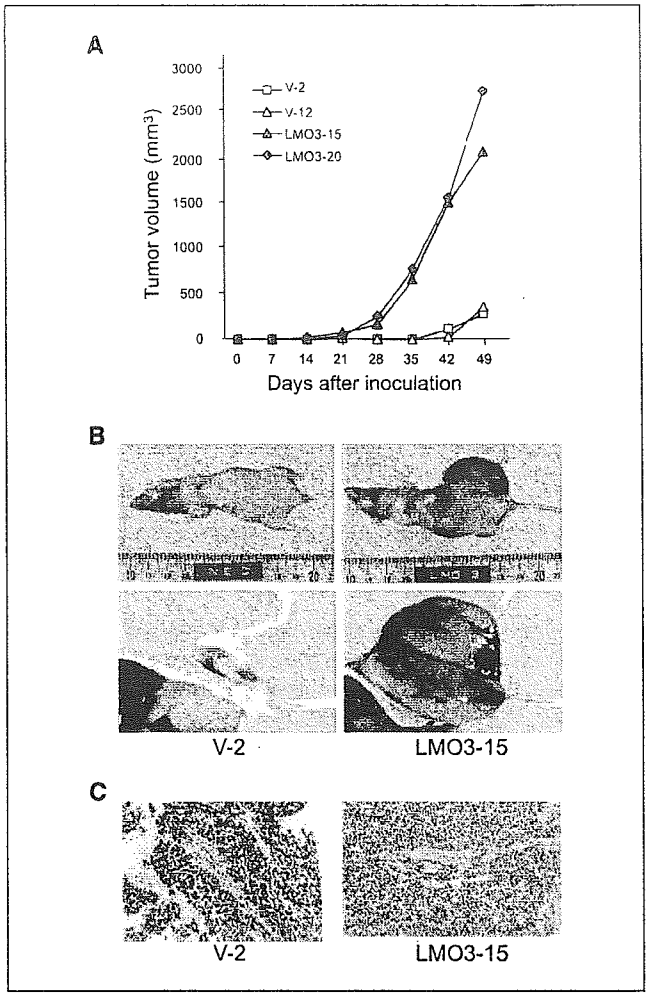

Figure 5. Tumor growth in nude mice. *A*, nude mice were injected s.c. with 5×10^6 of SH-SY5Y cells or the indicated stable transfectants and tumor volumes were estimated weekly. *Points*, mean of 8 to 11 independent tumors. *B*, photographs of the tumors 49 days after s.c. injection of V-2 (*left*) and LMO3-15 cells (*right*) into nude mice. *C*, paraffin sections of the tumors arising from V-2 (*left*) and LMO3-15 cells (*right*) were stained with H&E.

LMO3 physically interacts with HEN2. Because LMO3 and HEN2 were coexpressed in the majority of unfavorable neuroblastomas as well as neuroblastoma cell lines, we examined whether LMO3 could interact with HEN2 in mammalian cells. Whole cell lysates prepared from COS7 cells transfected with the expression plasmids for HA-tagged LMO3 and FLAG-tagged HEN2 were immunoprecipitated with the anti-HA or with the anti-FLAG antibody followed by immunoblotting with the anti-FLAG or with the anti-HA antibody, respectively. As shown in Fig. 3*A*, FLAG-HEN2 was coimmunoprecipitated with HA-LMO3. We then examined the subcellular distribution of LMO3 and

HEN2. COS7 cells were cotransfected with the expression plasmids for HA-LMO3 and FLAG-HEN2 and double stained with anti-HA and anti-FLAG antibodies. As shown in Fig. 3*B*, LMO3 as well as HEN2 appear exclusively nuclear. On closer inspection by merging two images, these two proteins colocalized in the nucleus. Consistent with the previous reports (35), HA-LMO3 was coimmunoprecipitated with FLAG-HEN1 under our experimental conditions (Fig. 3*C*).

Overexpression of LMO3 accelerates growth of SH-SY5Y neuroblastoma cells. We addressed the question whether LMO3 could induce cell growth of neuroblastoma. To this end, we transfected the expression plasmid for FLAG-LMO3-A or the empty plasmid into SH-SY5Y neuroblastoma cells and established two stable transfectants overexpressing FLAG-LMO3-A (named as LMO3-15 and LMO3-20). As shown in Fig. 4*A*, the expression levels of FLAG-LMO3-A were higher in LMO3-15 and LMO3-20 cells than in the parental SH-SY5Y and the control transfectants (V-2 and V-12). LMO3-15 expressed FLAG-LMO3-A at the level comparable with that in LMO3-20. Similar results were also obtained by RT-PCR analysis (Fig. 4*B*). No obvious morphologic changes could be observed in LMO3-15 and LMO3-20 cells (data not shown). As shown in Fig. 4*C*, LMO3-15 and LMO3-20 cells proliferated at a much faster rate than the control transfectants and SH-SY5Y cells in culture medium containing 10% serum. More importantly, LMO3-15 and LMO3-20 cells continued to grow exponentially even in the low serum culture medium, whereas the growth of the vector-transfected cells as well as SH-SY5Y cells was significantly suppressed under this condition.

To examine whether the LMO3-A-overexpressing cells have an ability to grow in soft agar medium, each transfectants were cultured in soft agar medium for 3 weeks. The numbers of colonies with diameters >300 μm formed by each transfectants in soft agar were scored. LMO3-15 and LMO3-20 cells formed large distinct colonies and showed a statistically significant increase in the number of colonies compared with the vector-transfected cells and SH-SY5Y cells (Fig. 4*D*). These results strongly suggest that overexpression of LMO3 is sufficient to induce malignant transformation in neuroblastoma cells. We also tried to obtain the cells stably transfected with HEN2 but never been successful with unknown reason.

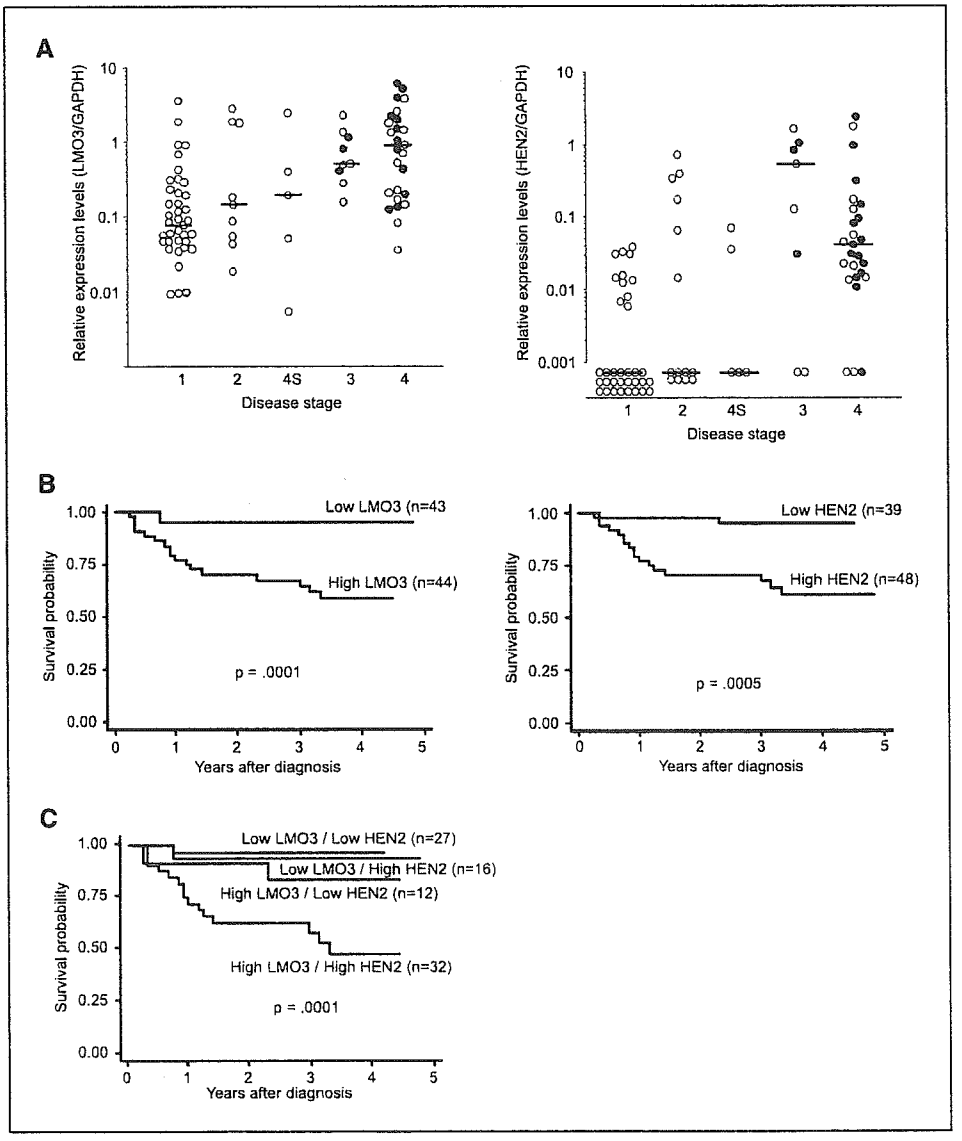

Figure 6. Expression of *LMO3* and *HEN2* mRNA in 87 primary neuroblastomas. *A*, expression levels of *LMO3* (*left*) and *HEN2* (*right*) transcripts in 87 primary neuroblastoma samples categorized by the patient's clinical stage were examined by a quantitative real-time RT-PCR. Relative expression levels of *LMO3* or *HEN2* mRNA were determined by calculating the ratio between *GAPDH* and *LMO3* or *HEN2*. *Bars*, median levels of *LMO3* or *HEN2* expression in each stage; *open* and *closed circles*, samples from patients who are alive and dead, respectively. *B* and *C*, Kaplan-Meier survival curves of patients with neuroblastomas based on high or low expression of *LMO3*, *HEN2* (*B*), or *LMO3* and *HEN2* (*C*).

LMO3 induces marked tumor growth in nude mice. SH-SY5Y cells with a single copy of *MYCN* form tumors in nude mice, although the growth rate is slow compared with that of the other neuroblastoma cell lines with *MYCN* amplification (38). To examine whether overexpression of LMO3 in SH-SY5Y cells could affect the tumor growth *in vivo*, we injected the each transfectants into the left flank of athymic nude mice, and the tumor volumes were measured weekly. V-2 and V-12 cells slowly formed tumors with similar kinetics and of similar sizes 35 to 42 days after injection (Fig. 5*A*). In contrast, the tumors grew rapidly in nude mice implanted with LMO3-15 or LMO3-20 cells. The sizes of the excised tumors from the LMO3-15-implanted mice on day 49 were >10-fold larger than those of control mice (Fig. 5*B*) and showed histologically undifferentiated neuroblastoma with small round cell shapes and small amounts of stromal components (Fig. 5*C*).

Expression of *LMO3* and *HEN2* is associated with a poor outcome of neuroblastoma. To verify whether a significant relationship could be observed between the expression of *LMO3* and/or *HEN2* in primary neuroblastomas and the patients' survival, we quantitatively measured the expression levels of *LMO3* and *HEN2* mRNA in 87 primary tumors by using a quantitative real-time RT-PCR. The values of the levels of *LMO3* and *HEN2* expression were normalized to that of *GAPDH* expression [relative expression values (REV)]. The high level of *LMO3* expression was significantly associated with high expression of *HEN2* (Student's *t* tests, mean ± SE: 1.43 ± 0.27 REV, n = 48 versus 0.54 ± 0.17 REV, n = 39; P = 0.001), older age (≥1-year-old: 1.37 ± 0.29, n = 32 versus <1-year-old: 0.84 ± 0.21, n = 55; P = 0.008), advanced disease stages (stages III + IV: 1.83 ± 0.35, n = 34 versus stages I + II + IVS: 0.52 ± 0.14; P < 0.00005; Fig. 6*A*), low levels of *TrkA* expression (low TrkA: 1.63 ± 0.34, n = 37 versus high *TrkA*: 0.59 ± 0.15, n = 50; P = 0.0003), *MYCN* amplification (amplification: 1.91 ± 0.44, n = 27 versus single copy: 0.64 ± 0.13, n = 60; P = 0.0002), and sporadic cases of neuroblastoma (sporadic: 1.68 ± 0.32, n = 39 versus mass screening: 0.51 ± 0.14, n = 48; P < 0.00005). The high level of *HEN2* expression was also significantly correlated with high expression of *LMO3* (χ^2 tests: P = 0.001), older age (P < 0.0005), advanced stages (P < 0.0005; Fig. 6*B*), low *TrkA* expression (P < 0.0005), *MYCN* amplification (P < 0.0005), and sporadic cases of neuroblastoma (P < 0.0005). Thus, high expression of *LMO3* and *HEN2* was well associated with conventional markers indicating the poor prognosis of neuroblastoma.

We next tested if expression levels of *LMO3* and *HEN2* could have prognostic significance in primary neuroblastomas. The results for log-rank tests showed that high expression of *LMO3* or *HEN2* was significantly associated with poor survival (P = 0.0002 and 0.0005, respectively; Fig. 6*C* and *D*). Remarkably, the combination of high expression of both *LMO3* and *HEN2* showed the significantly worse prognosis compared with the other combinations of *LMO3* and *HEN2* expression levels as shown in Fig. 6*E*. As expected, older patients and the patients with advanced tumors, low expression of *TrkA*, amplified *MYCN*, and the tumors found by mass screening were associated with short time to survival (P < 0.00005). However, the adrenal origin of the tumor was not associated with the outcome (P = 0.19; data not shown).

The univariate analysis suggested that *LMO3* expression (P < 0.0005), *HEN2* expression (P = 0.004), age (P < 0.0005), *MYCN* amplification (P < 0.0005), and mass screening (P = 0.001) were of prognostic importance, supporting the results of the log-rank test (Table 1). Furthermore, the multivariate analysis showed that

Table 1. Simple Cox regression models using LMO3 expression and dichotomous factors of HEN2 expression, age, MYCN amplification, mass screening, and origin (n = 87)

Model	Factor	P	Hazard ratio (95% confidence interval)
A	LMO3 expression (high vs low)	<0.0005	1.80 (1.32-2.47)
B	HEN2 expression (high vs low)	0.004	8.69 (2.00-37.7)
C	Age (≥1 vs <1 y)	<0.0005	8.75 (2.87-26.7)
D	MYCN amplification (1 copy vs >1 copy)	<0.0005	0.049 (0.014-0.171)
E	Mass screening (+ vs −)	0.001	0.032 (0.004-0.237)
F	Origin (adrenal gland vs others)	0.20	2.06 (0.684-6.23)

NOTE: All variables with two categories, except *LMO3* expression (log). Hazard ratio shows the relative risk of death of first category relative to the second. Because all patients with advanced tumor stages and low expression of *TrkA* had died of the tumor, a Cox regression model with the tumor stage or *TrkA* expression was not fitted.

Table 2. Multiple Cox regression models using LMO3 expression and dichotomous factors of HEN2 expression, age, MYCN amplification, mass screening, and origin (n = 87)

Model	Factor	P	Hazard ratio (95% confidence interval)
A	LMO3 expression (high vs low)	0.005	1.61 (1.16-2.23)
	HEN2 expression (high vs low)	0.029	5.32 (1.19-23.9)
B	LMO3 expression (high vs low)	0.005	1.62 (1.15-2.28)
	Age (>1 vs <1 y)	0.002	5.79 (1.86-18.1)
C	LMO3 expression (high vs low)	0.066	1.36 (0.98-1.89)
	MYCN amplification (1 copy vs >1 copy)	<0.0005	0.075 (.02-.282)
D	LMO3 expression (high vs low)	0.044	1.42 (1.01-2.01)
	Mass screening (+ vs −)	0.005	0.051 (0.007-0.404)
E	LMO3 expression (high vs low)	<0.0005	1.78 (1.31-2.41)
	Origin (adrenal gland vs others)	0.21	2.02 (0.666-6.12)

NOTE: All variables with two categories, except *LMO3* expression (log). Hazard ratio shows the relative risk of death of first category relative to the second.

LMO3 expression was significantly associated with survival after controlling *HEN2* expression ($P = 0.005$), age ($P = 0.005$), mass screening ($P = 0.044$), and origin ($P < 0.0005$), suggesting that *LMO3* expression was an independent prognostic factor from the other factors (Table 2). *LMO3* expression was marginally associated with survival after controlling *MYCN* amplification ($P = 0.066$). On the other hand, because *HEN2* expression was highly associated with age, *MYCN* amplification, and mass screening, it was not significantly associated with survival after controlling age, *MYCN* amplification, and mass screening in the corresponding multiple Cox regression models (data not shown).

Discussion

In the present study, we have identified that both *LMO3* and *HEN2* are expressed at higher levels in aggressive neuroblastomas especially with *MYCN* amplification than those with favorable prognosis. Coexpression of *LMO3* and *HEN2* has been observed almost exclusively in neuroblastoma cell lines, not the other lines, suggesting that their expression and function are neuronal specific. Furthermore, LMO3 physically interacted with HEN2 in mammalian cells. The functional significance of LMO3 expression was shown by a stable transfection into SH-SY5Y neuroblastoma cells, colony formation in soft agar, and tumor growth in nude mice, all of which have suggested that LMO3, probably by interacting with endogenous HEN2, markedly promotes the tumor growth. Indeed, the tumors with high expression of both *LMO3* and *HEN2* have shown the worst prognosis in the analysis of 87 primary neuroblastomas. Thus, our results suggested that, in concert with HEN2, the neuronal specifically expressed LMO3 plays an important role in the tumorigenesis of neuroblastoma. Our observation is strikingly intriguing because that *LMO1* or *LMO2* is already known to be the oncogene in T-cell acute lymphoblastic leukemia and that *LMO4* has recently been implicated in the genesis of breast cancer (4, 9).

We have identified a *Nbla3267/LMO3* clone from the screening of differentially expressed genes between favorable and unfavorable subsets of neuroblastoma. *LMO3* was one of the genes expressed at higher levels in the latter than the former (24), like *MYCN* oncogene and *DDX1*, a DEAD box gene coamplified with *MYCN* in aggressive neuroblastomas. In the development of hematopoietic system, LMO1 and LMO2 form a transcriptional complex with Ldb1, a LIM domain–binding protein, and a basic helix-loop-helix protein TAL1, which was identified as an oncogene at the translocation breakpoint in T-cell ALL (4–7). From the analogy with the LMO1 or LMO2 transcriptional machinery in T-cell ALL, we searched for the similar complex in the neuronal system by using the different subsets of primary neuroblastoma and the cell lines in comparison with the T-cell ALL cell lines. As a result, the neuronal-specific pattern of expression was observed in *LMO3*, *Ldb2*, *HEN1*, and *HEN2*, among which *LMO3* and *HEN2* were significantly highly expressed in the unfavorable subset of neuroblastomas with *MYCN* amplification compared with the favorable subset. This result strongly suggested that *LMO3* may function in collaboration with *HEN2* in advanced stages of neuroblastoma. Indeed, both genes were coexpressed only in neuroblastoma derived-cell lines, not in other tumor-derived ones, suggesting that their expression is lineage specific. Furthermore, LMO3 and HEN2 physically interacted in mammalian cells, albeit with weak interaction between LMO3 and HEN1 (35). Thus, these results also suggest that LMO3 and HEN2 form a neuronal cassette mimicking the hematopoietic complex composed of LMO2 and TAL1 and regulate the growth of neuroblastoma.

The neuronal-specific basic helix-loop-helix transcription factors, HEN1 and HEN2, were originally identified from the cDNA library of a neuroblastoma cell line based on cross-hybridization with TAL1 (14, 15). Their expression was restricted to the developing nervous system and a neuroblastoma cell line. However, their function has long been unclear. Recently, Bao et al. have reported that HEN1 interacts with LMO proteins by yeast two-hybrid screen and that *Xenopus* HEN1, in concert with XLMO3, is a critical regulator of neurogenesis (35). This prompted us to test our hypothesis both *in vitro* and *in vivo*. As the results, we found that the SH-SY5Y neuroblastoma cells stably overexpressing LMO3, presumably by acting with endogenous HEN2, gained rapid cell growth in the culture medium with 10% or 1% serum, in the soft agar medium, and in nude mice. These suggested that LMO3 is a neuronal-specific oncogene in neuroblastoma, without any rearrangement of the *LMO3* gene (data not shown). However, we failed to establish a stable SH-SY5Y cell line transfected with HEN2. It is presumed that overexpression of HEN2 might have caused cell death or growth arrest in the cells, albeit the reason is elusive.

The double transgenic mice overexpressing LMO2 and TAL1 displayed a more rapid development of leukemia compared with those overexpressing LMO2 alone, suggesting that LMO2 and TAL1 act synergistically through their complex formation in the development of leukemia (13). Of note, Ono et al. reported that LMO2 and TAL1 act as cofactors for GATA3 to induce the expression of the *retinaldehyde dehydrogenase 2* gene in T-cell ALL (39). On the other hand, a stable complex comprising LMO2, TAL1, and GATA1 was required to promote erythroid differentiation (32). Therefore, LMO3 and HEN2 may also form a nuclear complex, including family members of GATA to regulate cell growth and differentiation in neuroblastoma. Our preliminary data have suggested that GATA2, GATA3, GATA4, and GATA6 are highly expressed in neuroblastoma cell lines, among which GATA4 and GATA6 are predominantly coexpressed in neuroblastoma cell lines compared with T-cell ALL lines. Thus, LMO3 and HEN2, in collaboration with GATA and Ldb families, may play a role in determining cell fate in both neural development and neuroblastoma genesis, although this hypothesis needs to be elucidated. Recently, it has been shown that LMO3 enhanced the ability of HEN1 through the physical interaction to transactivate the expression of *Neurogenin-1* as well as *NeuroD* and thereby induced the neuronal differentiation in frog embryos (35). We tested if this is the case in the neuroblastoma cells. However, our preliminary results suggested that the LMO3/HEN2 complex does not transactivate the *Neurogenin-1* as well as *NeuroD* promoter in neuroblastoma cell lines,[5] although it is unclear if the complex could work in normal neuronal development. Thus, like LMO2, alterations in the LMO3-containing transcriptional complex might differentially regulate expression of the downstream target genes closely involved in neuronal differentiation or tumor formation.

[5] Unpublished data.

It is striking that high levels of expression of both *LMO3* and *HEN2* are significantly associated with the poor prognosis in primary neuroblastomas. This clearly reflects how importantly both genes are functioning in the progression of neuroblastoma *in vivo*. Of interest, expression of either gene is well correlated with *MYCN* amplification, raising the possibility that they might be the downstream targets of MYCN. However, we could not confirm it in human neuroblastoma cell line SH-EP in which MYCN was regulated under the control of the rTet-inducible expression system (40). In agreement with this, cDNA microarray-based screening for the genes induced in the *MYCN*-amplified neuroblastoma cells thus far failed to detect either LMO3 or HEN2 (41, 42). The link between LMO family molecules and the other oncogenes or tumor suppressor genes is also important. Despite the lack of prognostic significance, LMO4 overexpressed in breast cancer seems to be indispensable in the mammary carcinogenesis because it interacts with both BRCA1 and CtIP to repress the BRCA1 function (10). This suggests that, similarly to LMO4, LMO3 may also have the interacting partners related to the tumorigenesis. Thus, LMO3 and HEN2 as well as their associated molecules might be good candidates for the future targets of the therapy against aggressive neuroblastomas.

Acknowledgments

Received 12/28/2004; revised 3/9/2005; accepted 3/23/2005.

Grant support: Grant-in-Aid from the Ministry of Health, Labour and Welfare for Third Term Comprehensive Control Research for Cancer, Grant-in-Aid for Scientific Research on Priority Areas from the Ministry of Education, Culture, Sports, Science and Technology, Japan, and Grant-in-Aid for Scientific Research from Japan Society for the Promotion of Science. M. Aoyama is an awardee of the Research Resident Fellowship from the Foundation for Promotion of Cancer Research in Japan.

The costs of publication of this article were defrayed in part by the payment of page charges. This article must therefore be hereby marked *advertisement* in accordance with 18 U.S.C. Section 1734 solely to indicate this fact.

We thank S. Sakiyama for critical reading of the article; A. Morohashi, N. Kitabayashi, H. Murakami, and N. Sugimitsu for excellent technical assistance; and the following institutions and hospitals for supplying the tumor samples: Department of Pediatric Surgery, Iwaki Kyoritsu Hospital; Departments of Pediatrics and Pediatric Surgery, Aichi Medical University; Department of Pediatrics, Nara Hospital; Department of Pediatrics, Kyoto Prefectural University of Medicine; Department of Pediatric Surgery, Kimitsu Central Hospital; Department of Surgery, Gunma Children's Medical Center; Department of Pediatrics, Sapporo National Hospital; Departments of Pediatrics, Pediatric Surgery, and General Surgery, Jichi Medical School; Departments of Pediatrics and Pediatric Surgery, Kagoshima University; Department of Pediatrics, Juntendo University; Department of Pediatric Surgery, Showa University; Department of Pediatric Surgery, Niigata University; Departments of Surgery and Pathology, Chiba Children's Hospital; Department of Pediatric Surgery, Chiba University; Department of Pediatric Surgery, Osaka City General Hospital; Department of Pediatric Surgery, Tsukuba University; Department of Pediatric Surgery, Tokai University; Department of Surgery, Tokyo Metropolitan Kiyose Children's Hospital; Department of Pediatric Surgery, Tohoku University; Tumor Board, Hyogo Prefectural Kobe Children's Hospital; and First Department of Surgery, Hokkaido University.

References

1. Dawid IB, Breen JJ, Toyama R. LIM domains: multiple roles as adaptors and functional modifiers in protein interactions. Trends Genet 1998;14:156–62.
2. Sanchez-Garcia I, Rabbitts TH. The LIM domain: a new structural motif found in zinc-finger-like proteins. Trends Genet 1994;10:315–20.
3. Dawid IB, Toyama R, Taira M. LIM domain proteins. C R Acad Sci III 1995;318:295–306.
4. Rabbitts TH. LMO T-cell translocation oncogenes typify genes activated by chromosomal translocations that alter transcription and developmental processes. Genes Dev 1998;12:2651–7.
5. McGuire EA, Rintoul CE, Sclar GM, Korsmeyer SJ. Thymic overexpression of Ttg-1 in transgenic mice results in T-cell acute lymphoblastic leukemia/lymphoma. Mol Cell Biol 1992;12:4186–96.
6. Fisch P, Boehm T, Lavenir I, et al. T-cell acute lymphoblastic lymphoma induced in transgenic mice by the RBTN1 and RBTN2 LIM-domain genes. Oncogene 1992;7:2389–97.
7. Neale GA, Rehg JE, Goorha RM. Disruption of T-cell differentiation precedes T-cell tumor formation in LMO-2 (rhombotin-2) transgenic mice. Leukemia 1997;3:289–90.
8. Kenny DA, Jurata LW, Saga Y, Gill GN. Identification and characterization of LMO4, an LMO gene with a novel pattern of expression during embryogenesis. Proc Natl Acad Sci U S A 1998;95:11257–62.
9. Visvader JE, Venter D, Hahm K, et al. The LIM domain gene LMO4 inhibits differentiation of mammary epithelial cells *in vitro* and is overexpressed in breast cancer. Proc Natl Acad Sci U S A 2001;98:14452–7.
10. Sum EY, Peng B, Yu X, et al. The LIM domain protein LMO4 interacts with the cofactor CtIP and the tumor suppressor BRCA1 and inhibits BRCA1 activity. J Biol Chem 2002;277:7849–56.
11. Foroni L, Boehm T, White L, et al. The rhombotin gene family encode related LIM-domain proteins whose differing expression suggests multiple roles in mouse development. J Mol Biol 1992;226:747–61.
12. Wadman I, Li J, Bash RO, et al. Specific *in vivo* association between the bHLH and LIM proteins implicated in human T cell leukemia. EMBO J 1994;13:4831–9.
13. Larson RC, Lavenir I, Larson TA, et al. Protein dimerization between Lmo2 (Rbtn2) and Tal1 alters thymocyte development and potentiates T cell tumorigenesis in transgenic mice. EMBO J 1996;15:1021–7.
14. Brown L, Espinosa R III, Le Beau MM, Siciliano MJ, Baer R. HEN1 and HEN2: a subgroup of basic helix-loop-helix genes that are coexpressed in a human neuroblastoma. Proc Natl Acad Sci U S A 1992;89:8492–6.
15. Begley CG, Lipkowitz S, Gobel V, et al. Molecular characterization of NSCL, a gene encoding a helix-loop-helix protein expressed in the developing nervous system. Proc Natl Acad Sci U S A 1992;89:38–42.
16. Brodeur GM, Azar C, Brother M, et al. Effect of genetic factors on prognosis and treatment. Cancer 1992;70:1685–94.
17. Brodeur GM, Nakagawara A. Molecular basis of clinical heterogeneity in neuroblastoma. J Pediatr Hematol Oncol 1992;14:111–6.
18. Brodeur GM, Seeger RC, Schwab M, Varmus HE, Bishop JM. Amplification of N-*myc* in untreated human neuroblastomas correlates with advanced disease stage. Science 1984;224:1121–4.
19. Seeger RC, Brodeur GM, Sather H, et al. Association of multiple copies of the N-*myc* oncogene with rapid progression of neuroblastomas. N Engl J Med 1985;313:1111–6.
20. Nakagawara A, Arima M, Azar CG, Scavarda NJ, Brodeur GM. Inverse relationship between trk expression and N-*myc* amplification in human neuroblastomas. Cancer Res 1992;52:1364–8.
21. Nakagawara A, Arima-Nakagawara M, Scavarda NJ, Azar CG, Cantor AB, Brodeur GM. Association between high levels of expression of the TRK gene and favorable outcome in human neuroblastoma. N Engl J Med 1993;328:847–54.
22. Gross N, Beretta C, Peruisseau G, Jackson D, Simmons D, Beck D. CD44H expression by human neuroblastoma cells: relation to MYCN amplification and lineage differentiation. Cancer Res 1994;54:4238–42.
23. Berwanger B, Hartmann O, Bergmann E, et al. Loss of a FYN-regulated differentiation and growth arrest pathway in advanced stage neuroblastoma. Cancer Cell 2002;2:377–86.
24. Ohira M, Morohashi A, Inuzuka H, et al. Expression profiling and characterization of 4200 genes cloned from primary neuroblastomas: identification of 305 genes differentially expressed between favorable and unfavorable subsets. Oncogene 2003;22:5525–36.
25. Ohira M, Shishikura T, Kawamoto T, et al. Hunting the subset-specific genes of neuroblastoma: expression profiling and differential screening of the full-length-enriched oligo-capping cDNA libraries. Med Pediatr Oncol 2000;35:547–9.
26. Brodeur GM, Pritchard J, Berthold F, et al. Revisions of the international criteria for neuroblastoma diagnosis, staging, and response to treatment. J Clin Oncol 1993;11:1466–77.
27. Matsumura T, Iehara T, Sawada T, Tsuchida Y. Prospective study for establishing the optimal therapy of infantile neuroblastoma in Japan. Med Pediatr Oncol 1998;31:210.
28. Kaneko M, Nishihira H, Mugishima H, et al.; Study Group of Japan for Treatment of Advanced Neuroblastoma, Tokyo, Japan. Stratification of treatment of stage 4 neuroblastoma patients based on N-*myc* amplification status. Med Pediatr Oncol 1998;31:1–7.
29. Takihara Y, Tomotsune D, Shirai M, et al. Targeted disruption of the mouse homologue of the *Drosophila* polyhomeotic gene leads to altered anteroposterior patterning and neural crest defects. Development 1997;124:3673–82.
30. Agulnick AD, Taira M, Breen JJ, Tanaka T, Dawid IB, Westphal H. Interactions of the LIM-domain-binding factor Ldb1 with LIM homeodomain proteins. Nature 1996;384:270–2.
31. Jurata LW, Kenny DA, Gill GN. Nuclear LIM interactor, a rhombotin and LIM homeodomain interacting protein, is expressed early in neuronal development. Proc Natl Acad Sci U S A 1996;93:11693–8.
32. Bach I, Carriere C, Ostendorff HP, Andersen B, Rosenfeld MG. A family of LIM domain-associated cofactors confer transcriptional synergism between LIM and Otx homeodomain proteins. Genes Dev 1997;11:1370–80.
33. Osada H, Grutz G, Axelson H, Forster A, Rabbitts TH. Association of erythroid transcription factors: complexes involving the LIM protein RBTN2 and the zinc-finger protein GATA1. Proc Natl Acad Sci U S A 1995;92:9585–9.
34. Valge-Archer VE, Osada H, Warren AJ, et al. The LIM protein RBTN2 and the basic helix-loop-helix protein TAL1 are present in a complex in erythroid cells. Proc Natl Acad Sci U S A 1994;91:8617–21.
35. Bao J, Talmage DA, Role LW, Gautier J. Regulation of neurogenesis by interactions between HEN1 and neuronal LMO proteins. Development 2000;127:425–35.